bioRxiv preprint doi: https://doi.org/10.1101/2021.05.21.445201; this version posted June 9, 2021. The copyright holder for this preprint (which was not certified by peer review) is the author/funder. All rights reserved. No reuse allowed without permission.

Evidence for Deleterious Antigenic Imprinting in SARS-CoV-2 Immune Response

Sanjana R. Sen[1], Emily C. Sanders[2], Alicia M. Santos[2], Keertna Bhuvan[2], Derek Y. Tang[2], Aidan A. Gelston[2], Brian M. Miller[2], Joni L. Ricks-Oddie[3,4] and Gregory A. Weiss[1,2,5]*

Author Affiliations:

[1] Department of Molecular Biology & Biochemistry, University of California, Irvine, Irvine CA 92697-3900 USA
[2] Department of Chemistry, University of California, Irvine, Irvine CA 92697-2025 USA
[3] Center for Statistical Consulting, Department of Statistics, University of California, Irvine, Irvine CA 92697-1250 USA
[4] Biostatics, Epidemiology and Research Design Unit, Institute for Clinical and Translational Sciences, University of California, Irvine, Irvine CA 92697-4094 USA
[5] Department of Pharmaceutical Sciences, University of California, Irvine, Irvine CA 92697-3958 USA

* Address correspondence to gweiss@uci.edu

Corresponding Author:

*GAW e-mail: gweiss@uci.edu, Tel: +1-949-824-5566, address: 1102 Natural Sciences 2, Irvine, CA 92697-2025, USA

Author Contributions:

S.R.S., and G.A.W. designed research; S.R.S., E.C.S., A.M.S., K.B., D.Y.T, A.A.G., and B.M.M. performed research; S.R.S., E.C.S. and G.A.W. analyzed data; J.L.R. advised on statistical analysis; S.R.S. and G.A.W. wrote the manuscript.

Competing Interests:

None.

Acknowledgements:

We thank Professor Elizabeth Bess and Professor Stacey Schultz-Cherry for helpful conversations, Kristin Gabriel for initial bioinformatics analysis, and the patients who generously donated their plasma samples (IRB# 2012-8716). We gratefully acknowledge the support of the UCI COVID-19 Basic, Translational and Clinical Research Fund (CRAFT), the Allergan Foundation, and UCOP Emergency COVID-19 Research Seed Funding. A.M.S thank the Minority Access to Research Careers (MARC) Program, funded by the NIH (GM-69337). J.L.R.-O. was supported by the National Center for Research Resources and the National Center for Advancing Translational Sciences from the NIH (TR001414).

bioRxiv preprint doi: https://doi.org/10.1101/2021.05.21.445201; this version posted June 9, 2021. The copyright holder for this preprint (which was not certified by peer review) is the author/funder. All rights reserved. No reuse allowed without permission.

Abstract

A previous report demonstrated the strong association between the presence of antibodies binding to an epitope region from SARS-CoV-2 nucleocapsid, termed Ep9, and COVID-19 disease severity. Patients with anti-Ep9 antibodies (Abs) had hallmarks of antigenic imprinting (AIM), including early IgG upregulation and cytokine-associated injury. Thus, the immunological memory of a previous infection was hypothesized to drive formation of suboptimal anti-Ep9 Abs in severe COVID-19 infections. This study identifies a putative primary antigen capable of stimulating production of cross-reactive, anti-Ep9 Abs. Binding assays with patient blood samples directly show cross-reactivity between Abs binding to Ep9 and only one bioinformatics-derived, homologous potential antigen, a sequence derived from the neuraminidase protein of H3N2 Influenza A virus. This cross-reactive binding is highly influenza strain specific and sensitive to even single amino acid changes in epitope sequence. The neuraminidase protein is not present in the influenza vaccine, and the anti-Ep9 Abs likely resulted from the widespread influenza infection in 2014. Therefore, AIM from a previous infection could underlie some cases of COVID-19 disease severity.

Importance

Infections with SARS-COV-2 result in diverse disease outcomes, ranging from asymptomatic to fatal. The mechanisms underlying different disease outcomes remain largely unexplained. Previously, our laboratory identified a strong association between the presence of an antibody and increased disease severity in a subset of COVID-19 patients. Here, we report that this severity-associated antibody cross-reacts with viral proteins from an influenza A viral strain from 2014. Therefore, we speculate that antibodies generated against previous infections, like the 2014 influenza A, play a significant role in directing some peoples' immune responses against SARS-COV-2. Such understanding of the sources and drivers of COVID-19 disease severity can help early identification and pre-emptive treatment.

bioRxiv preprint doi: https://doi.org/10.1101/2021.05.21.445201; this version posted June 9, 2021. The copyright holder for this preprint (which was not certified by peer review) is the author/funder. All rights reserved. No reuse allowed without permission.

Introduction

Original antigenic sin or antigenic imprinting (AIM) occurs when the immune response adapted for a primary (or "original") infection instead targets a similar, but not identical, pathogen[1]. Since B-cells undergo affinity maturation post-primary infection, cross-reactive Abs from previous infections can outcompete naïve Abs[2]. AIM ideally accelerates pathogen clearance by targeting highly conserved antigens; however, suboptimal targeting by non-neutralizing, Ab binding can exacerbate disease[2]. The range of outcomes observed in COVID-19, from asymptomatic to fatal, could result from a patient's immunological memory[1,3].

Ab cross-reactivity from AIM causes a wide range of disease outcomes. For example, some Abs from healthy individuals previously exposed to other common human coronaviruses (hCoV) could cross-react with SARS-CoV-2 spike protein to neutralize viral pseudotypes[4]. However, other prepandemic Abs with cross-reactivity to SARS-CoV-2 nucleocapsid (NP) and spike proteins did not protect against severe symptoms [5]. Humoral immunity to hCoVs, NL63 and 229E[6], respiratory syncytial virus, cytomegalovirus and herpes simplex virus-1[7,8] has been associated with more severe COVID-19 disease.

The presence of Abs with affinity for a 21-mer peptide derived from SARS-CoV-2 NP, an epitope region termed Ep9, have been correlated with severe COVID-19. The patients, termed αEp9(+), comprised ≈27% of the sampled, SARS-CoV-2-infected population (n = 186). The αEp9(+) patients (n = 34) had high, early levels of αN IgGs, typically within the first week, compared to αEp9(-) patients; αEp9(+) individuals also experienced cytokine-related, immune hyperactivity[9]. These two observations suggest an AIM-based mechanism for the disease severity observed in αEp9(+) patients. Here, we explore the epitope homology landscape and αEp9 Ab cross-reactivity to potentially identify an original antigen driving Ab-based immune response in αEp9(+) patients.

bioRxiv preprint doi: https://doi.org/10.1101/2021.05.21.445201; this version posted June 9, 2021. The copyright holder for this preprint (which was not certified by peer review) is the author/funder. All rights reserved. No reuse allowed without permission.

Results and Discussion

Assays measured levels of αEp9 IgGs and IgMs from αEp9(+) patients whose plasma was collected at various times post-symptom onset (PSO). Consistent with the hallmarks of AIM tracing a prior infection, αEp9 IgG levels appeared elevated as early as one day PSO in one patients. Similar IgG levels were observed in the patient population over >4 weeks (one-way ANOVA, $p = 0.321$); thus, αEp9 IgG started high and remained high. Levels of αEp9 IgMs amongst patients at various times PSO were also similar (one-way ANOVA, $p = 0.613$). The signals measured for αEp9 IgM levels were significantly lower than the equivalent αEp9 IgG levels (t-test, $p = 0.0181$) (Figure S1A); this difference could reflect lower IgM affinity, quantity, or both.

Searches for sequence and structural homologs of Ep9 using pBLAST[10] and VAST[11] databases suggested candidate primary antigens. A structural homolog from betaherpesvirus 6A and 14 other Ep9 sequence homologs were identified. Additionally, Ep9-orthologous regions from six human coronaviruses (SARS-CoV, MERS, OC43, HKU-1, NL63, 229E) were chosen for subsequent assays (Figure 1A, and Table S1). To expedite the binding measurements, the potential AIM epitope regions were subcloned into phagemids encoding the sequences as fusions to the M13 bacteriophage P8 coat protein. DNA sequencing and ELISA experiments demonstrated successful cloning and consistent phage display, respectively. Two epitopes failed to display on phage and were omitted from subsequent investigation (Table S2 and Figure S2A).

Phage ELISAs tested binding by Ep9 homologs to αEp9 Abs. An average response within the patient population was assessed using pooled plasma from three sets of five αEp9(+) and five αEp9(-) COVID-19 patients coated onto ELISA plates. Plasma from healthy individuals provided an additional negative control. Confirming previously reported results, SARS-COV-2 Ep9 and a homologous epitope from SARS-CoV-1 (90% similarity) bound only to plasma from αEp9(+) patients[9]. The αEp9 Ab affinity for SARS-CoV-1 is unlikely to drive SARS-CoV-2 AIM due to the former's limited spread in the US[12].

bioRxiv preprint doi: https://doi.org/10.1101/2021.05.21.445201; this version posted June 9, 2021. The copyright holder for this preprint (which was not certified by peer review) is the author/funder. All rights reserved. No reuse allowed without permission.

The panel of potential epitopes revealed a candidate epitope from the neuraminidase (NA) protein of an H3N2 influenza A strain, which circulated in 2014 (A/Para/128982-IEC/2014, Accession No. AIX95025.1), termed EpNeu here. The plasma from αEp9(+), but not αEp9(-) patients nor healthy individuals, bound EpNeu ($p<0.0001$, two-way ANOVA *ad hoc* Tukey test) (Figure 1C, D). Though Ep9 and EpNeu share 38% amino acid sequence similarity, other candidate epitope regions with significantly higher homology failed to bind to αEp9(+) plasma (Table S1).

Next, the specificity of αEp9 Abs binding to NA from different viral strains was explored. EpNeu provided a template for further homolog searches in sequence databases. Closely aligned NA sequences isolated from human, avian, and swine hosts in North America were chosen for further analysis (Figure 1F, Table S1). The sequences were phage-displayed as before. Despite their close similarity to EpNeu (up to 92.3% similarity or only one residue difference), none of the EpNeu homologs bound to Abs from αEp9(+) patients (Figure 1E). A single EpNeu amino acid substitution, K142N (numbering from full-length NA, Accession No. AID57909.1) in an H1N2 swine flu (2016) dramatically decreased binding affinity to Abs from αEp9(+) patients ($p<0.0001$ one-way ANOVA *ad hoc* Tukey). An epitope H4N6 avian influenza A (2010) missing residue S141, but including conserved K142, also greatly reduced binding to Abs from αEp9(+) patients ($p<0.0001$ one-way ANOVA *ad hoc* Tukey) (Figure 1E, 1F). Therefore, S141 and K142 are critical for binding to αEp9 Abs.

Do Ep9 and EpNeu epitopes bind the same Abs? Data from 34 αEp9(+) patients demonstrated a strong, highly significant correlation between levels of Abs binding to Ep9 and EpNeu epitopes in patient plasma (Figure 2A). Cross-reactivity was confirmed by a sandwich-format assay requiring bivalent, simultaneous binding to both eGFP-fused Ep9 and phage-displayed EpNeu (Figure 2B, S3). Cross-reactive Ab binding both Ep9 and EpNeu epitopes in

bioRxiv preprint doi: https://doi.org/10.1101/2021.05.21.445201; this version posted June 9, 2021. The copyright holder for this preprint (which was not certified by peer review) is the author/funder. All rights reserved. No reuse allowed without permission.

pooled plasma from αEp9(+) patients, but not in αEp9(-) patients with other αNP Abs or healthy donors was demonstrated. Thus, we conclude that αEp9 Abs also recognize the EpNeu epitope.

We then investigated whether EpNeu could present a viable antigen during infection with 2014 H3N2 (NCBI: txid1566483). Linear epitope analysis of full-length NA protein (Bepipred 2.0)[13] predicted a candidate antigen with eight residues from EpNeu, including S141 and K142, and ten additional residues (146-155). This predicted epitope region, termed EpPred, includes the conserved catalytic NA residue D151 targeted for viral neutralization by the immune system[14] (Figures 2C, and S4A). A model structure of 2014 H3N2 NA from Swiss-Model[15] and structural epitope prediction (Discotope 2.0)[16] also identified potential epitopes within EpPred (Figures 2C, D and S4B).

eGFP-fused EpPred (Figure S2B) was assayed with pooled plasma from five αEp9(+) patients. Controls included EpNeu and Ep9 (positive) and eGFP FLAG (negative). The αEp9 Abs bound to Ep9 with ≈2-fold stronger apparent affinity than for EpNeu (Figure 2E). The increased binding strength of Ep9 could result from additional rounds of Ab affinity maturation after the primary infection[2]. The longer length EpPred modestly improved upon the binding of EpNeu to αEp9 Abs (Figure 3C). Thus, αEp9 Abs likely target a larger epitope of H3N2 2014 NA beyond regions homologous to Ep9; full-length NA's balkiness to overexpression makes this difficult to test[17]. Additionally, the bacterially overexpressed epitopes assayed here do not include post-translational modifications. Taken together, the results support the hypothesis that αEp9 Abs found in severe COVID-19 disease can result from AIM with H3N2 influenza A. Unfortunately, patient histories typically do not include influenza infections and vaccinations. Isolated from Para, Brazil, the H3N2 2014 strain has unknown spread in North America. However, a severe outbreak of influenza A was recorded in 2014[18,19]. Since only hemagglutinin was sequenced for strain identification in 2014[19], the candidate AIM strain from the current investigation could not be effectively traced as only its NA sequence was available. Notably, the EpNeu homolog from the

bioRxiv preprint doi: https://doi.org/10.1101/2021.05.21.445201; this version posted June 9, 2021. The copyright holder for this preprint (which was not certified by peer review) is the author/funder. All rights reserved. No reuse allowed without permission.

2014 vaccine H3N2 strain (identical to Flu A 2015 H3N2 NA, Accession No. ANM97445.1) does not bind αEp9 Abs (Figure 1 E, F). Therefore, αEpNeu Abs must have been generated against a primary influenza infection, not the vaccine.

This report offers a molecular mechanism for AIM underlying the high-rate of severe COVID-19 in αEp9(+) patients. Specifically, we demonstrate cross-reactive binding between αEp9 Abs and a predicted NA epitope from a 2014 influenza A strain. Future studies could examine correlation between a country's rate of the H3N2 2014 influenza and severe COVID-19. Additionally, correlation could be tested using health systems that record influenza infections. Examining epitope conservation and Ab cross-reactivity could predict AIM-based immune responses and disease outcomes in future infections. Identifying detrimental, benign or beneficial AIM pathways could also guide vaccine design.

bioRxiv preprint doi: https://doi.org/10.1101/2021.05.21.445201; this version posted June 9, 2021. The copyright holder for this preprint (which was not certified by peer review) is the author/funder. All rights reserved. No reuse allowed without permission.

Figures (main text)

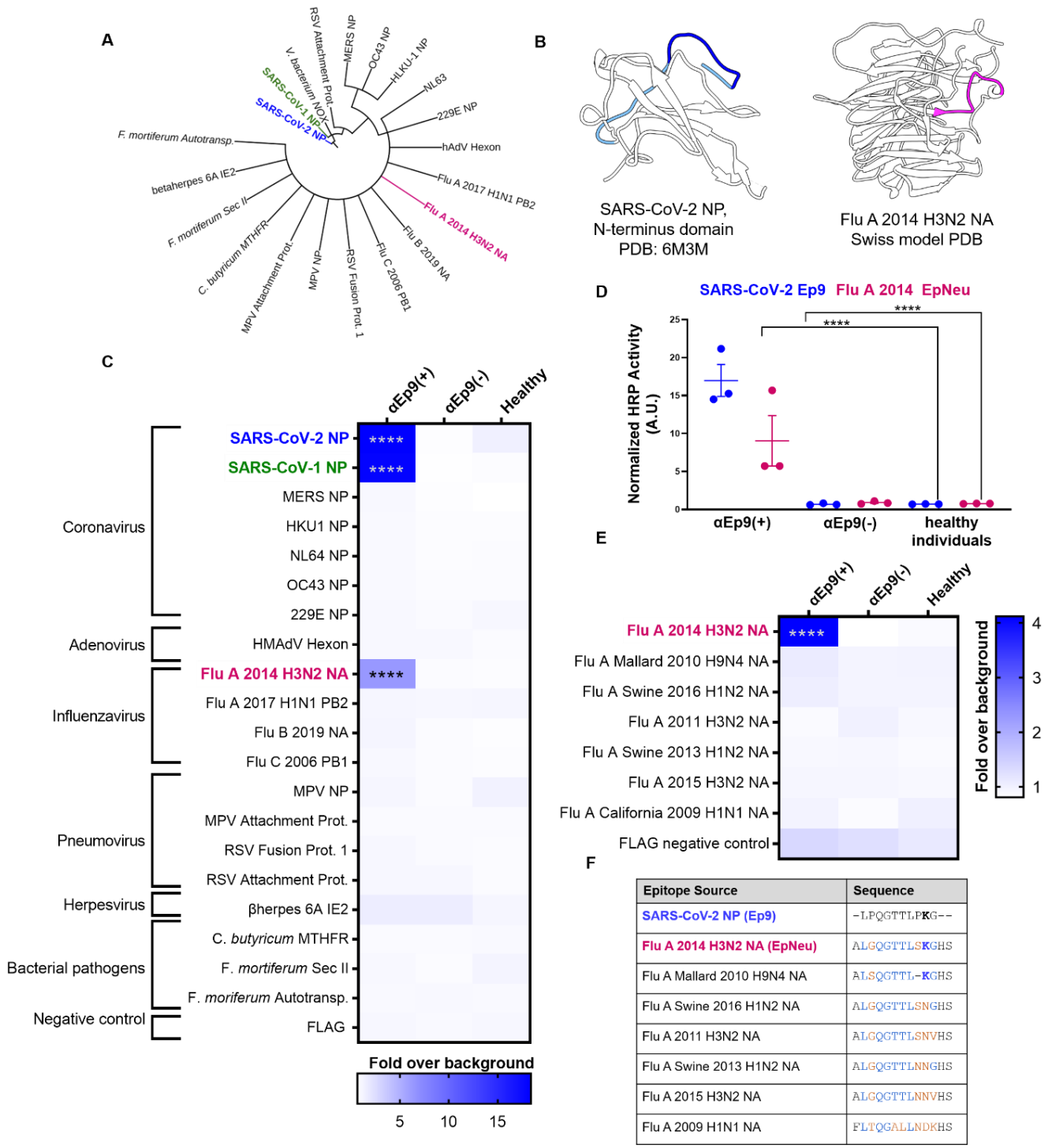

Epitope Source	Sequence
SARS-CoV-2 NP (Ep9)	-LPQGTTLPKG--
Flu A 2014 H3N2 NA (EpNeu)	ALGQGTTLSKGHS
Flu A Mallard 2010 H9N4 NA	ALSQGTTL-KGHS
Flu A Swine 2016 H1N2 NA	ALGQGTTLSNGHS
Flu A 2011 H3N2 NA	ALGQGTTLSNVHS
Flu A Swine 2013 H1N2 NA	ALGQGTTLNNGHS
Flu A 2015 H3N2 NA	ALGQGTTLNNVHS
Flu A 2009 H1N1 NA	FLTQGALLNDKHS

Figure 1 | Potential OAS epitopes for binding αEp9 Abs suggested by bioinformatics and tested by phage ELISA. (**A**) Cladogram depicting sequence homology of the Ep9 sequence from

bioRxiv preprint doi: https://doi.org/10.1101/2021.05.21.445201; this version posted June 9, 2021. The copyright holder for this preprint (which was not certified by peer review) is the author/funder. All rights reserved. No reuse allowed without permission.

SARS-CoV-2 to the bioinformatics-identified, closest homologs. Sequence alignments used pBLAST and VAST, and the cladogram was generated by iTOL [20]. (**B**) Structures of SARS-CoV-2 NP RNA binding domain (PDB: 6M3M) and the Flu A 2014 H3N2 NA protein (modeled by SWISS-Model [21]). SARS-CoV-2 NP highlights Ep9 residues (light and dark blue) and the region homologous region to EpNeu (dark blue). The depicted model of Flu A 2014 H3N2 NA highlights the EpNeu putative antigen (pink). (**C**) ELISAs examined binding of phage-displayed potential OAS epitopes to Abs from three sets of pooled plasma from five αEp9(+) patients, or five αEp9(-) patients. Pooled plasma from healthy patients was an additional negative control. The colors of the heat map represent the mean binding signal normalized to phage background negative controls (signal from phage without a displayed peptide). (**D**) Expansion of data from panel C shows ELISA signals from the independently assayed individual pools shows results from the individual pools (****p <0.0001 for a two-way ANOVA comparing binding of phage-displayed epitopes listed in panel C to different groups of pooled plasma, *ad hoc* Tukey test). (**E**) Using EpNeu as the search template to generate homologous sequences (shown in next panel), ELISAs examined EpNeu homologs' binding to pooled plasma from αEp9(+), αEp9(-), or healthy individuals. The data are represented as described in panel C (****p <0.0001 for two-way ANOVA c phage-displayed epitopes, *ad hoc* Tukey and Dunnett's test as shown). (**F**) Amino acid sequence alignment of the closely related Flu A NA homologs of EpNeu from pBLAST. Blue and orange residues represent conserved and mismatched amino acids, respectively, relative to Ep9. Bolded residues are important for epitope recognition by αEp9 Abs. Here, the term Flu refers to influenza.

bioRxiv preprint doi: https://doi.org/10.1101/2021.05.21.445201; this version posted June 9, 2021. The copyright holder for this preprint (which was not certified by peer review) is the author/funder. All rights reserved. No reuse allowed without permission.

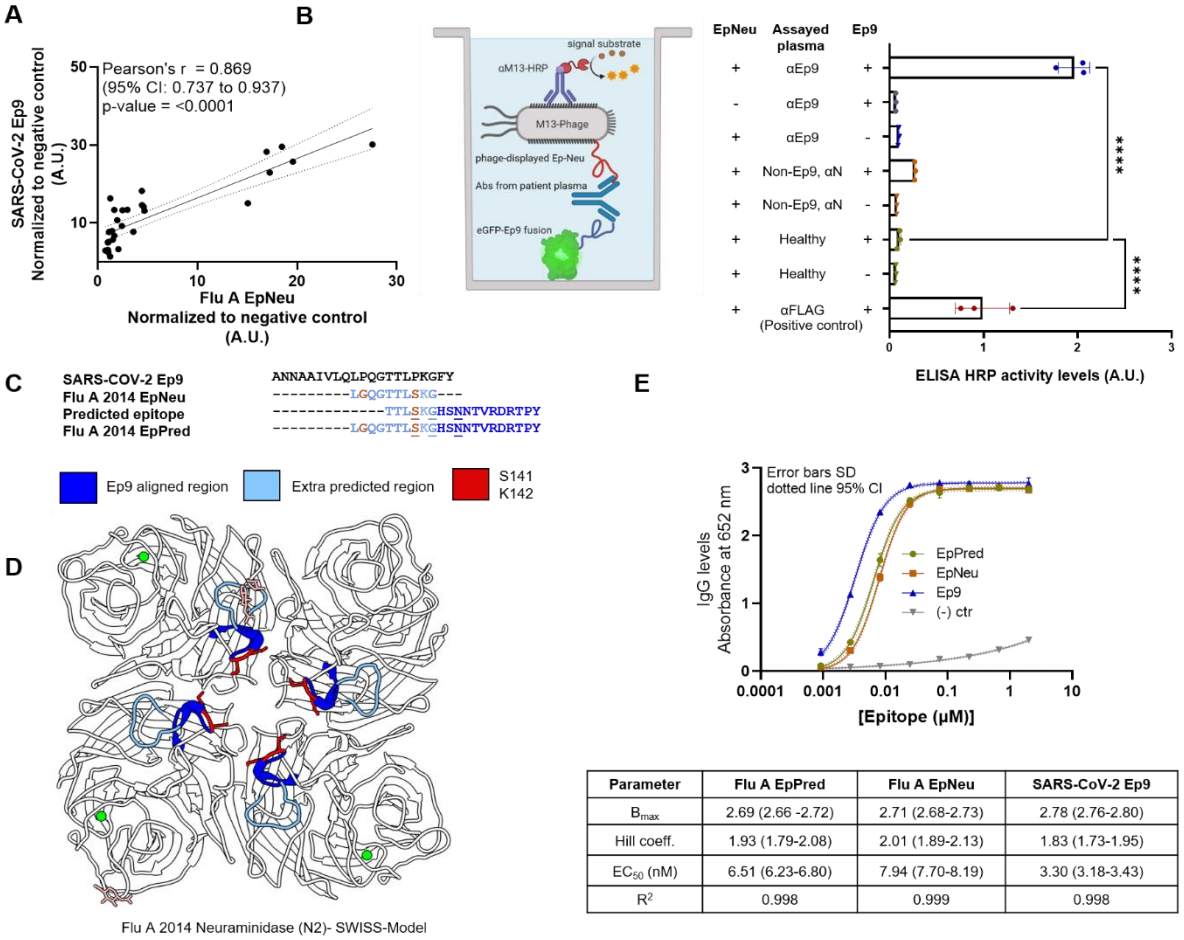

Parameter	Flu A EpPred	Flu A EpNeu	SARS-CoV-2 Ep9
B_{max}	2.69 (2.66 -2.72)	2.71 (2.68-2.73)	2.78 (2.76-2.80)
Hill coeff.	1.93 (1.79-2.08)	2.01 (1.89-2.13)	1.83 (1.73-1.95)
EC_{50} (nM)	6.51 (6.23-6.80)	7.94 (7.70-8.19)	3.30 (3.18-3.43)
R^2	0.998	0.999	0.998

Figure 2 | Cross-reactive Ab binding to both Ep9 and EpNeu, and EpNeu epitope prediction. (A) Comparing normalized levels of phage-displayed Ep9 and EpNeu binding to plasma-coated wells from individual αEp9(+) patients (n = 34). A strong correlation is observed, as shown by the depicted statistics. Each point in panels A through C represents data from individual patients. (**B**) A schematic diagram of the sandwich ELISA to examine cross-reactivity of αEp9 Abs. The assay tests for bivalent Ab binding to both Ep9 and EpNeu. Pooled plasma from five αEp9(+) patients or five αEp9(-) patients with other αNP Abs was tested for bivalent binding to both eGFP-fused Ep9 and phage-displayed EpNeu. Healthy patient plasma was used as a negative control. For additional negative controls, phage-FLAG and eGFP-FLAG replaced Ep9 and EpNeu, respectively (****p <0.0001 one-way ANOVA, *ad hoc* Tukey and Dunnett's test shown, with healthy plasma in the presence of EpNeu and Ep9 as negative control). Error bars represent SD. Individual points on bar graph represent technical replicates. (**C**) Linear and structural B-cell epitope prediction tools Bepipred 2.0 and Discotope 2.0 suggested an extended, linear epitope region from the influenza A H3N2 2014 NA, including the eight residues of Ep9 Neu (light blue) with an additional ten, C-terminal residues (dark blue). This extended, predicted epitope is termed EpPred. Structural epitope predictions are underlined. Residues on EpNeu that are not aligned with Ep9 are depicted in orange. (**D**) Structural model depicting the influenza A H3N2 2014 NA.

bioRxiv preprint doi: https://doi.org/10.1101/2021.05.21.445201; this version posted June 9, 2021. The copyright holder for this preprint (which was not certified by peer review) is the author/funder. All rights reserved. No reuse allowed without permission.

The model was generated using SWISS-Model based on the NA structure from influenza A H3N2 Tanzania 2010 (PDB: 4GZS). The NA structure highlights the EpNeu region (light blue), the extended residues in EpPred (dark blue), potential glycosylation sites (light pink), and the residues S141 and K142 (red), which are important for αEp9 Ab recognition. (**E**) Dose-dependent ELISA comparing binding of αEp9 Abs to Ep9, EpNeu and EpPred. Pooled plasma from five αEp9(+) patients and five αEp9(-) patients were tested in triplicates with varying concentrations of eGFP-fused epitopes. The data demonstrates the strongest interactions occurred between αEp9 Abs and Ep9 with an approximately 2-fold decrease in αEp9 Abs binding affinity for EpNeu. EpPred bound slightly stronger to αEp9 Abs than EpNeu; the difference in trend lines of EpNeu and EpPred are statistically significant ($p<0.0001$, Comparison of Fits). Trendlines represent non-linear regression fit with Hill slope analysis.

bioRxiv preprint doi: https://doi.org/10.1101/2021.05.21.445201; this version posted June 9, 2021. The copyright holder for this preprint (which was not certified by peer review) is the author/funder. All rights reserved. No reuse allowed without permission.

Supplementary Materials

Materials and Methods

Sequence and structural alignment analysis

To identify possible sources of primary infection responsible for αEp9 Ab generation, sequence and structural alignment with Ep9 residues and the SARS-CoV-2 NP was conducted. Alignment of Ep9 sequence with the orthologs from other human coronaviruses (hCoVs) such as SARS-CoV, MERS, HKU-1, NL63, 229E and OC43 was conducted using the Benchling sequence alignment tool [22] (https://benchling.com). To explore a wider range of human host pathogens pBLAST [10] (https://blast.ncbi.nlm.nih.gov/Blast.cgi) was used to search for Ep9 homology in a database of non-redundant protein sequences; common human-host viruses were specified in the organism category. The queries were conducted with the blastp (protein-protein BLAST) program [10] with search parameters automatically adjusted for short input sequences. Alignments spanning >7 residues were included here. The Vector Alignment Search Tool (VAST) [11] (https://structure.ncbi.nlm.nih.gov/Structure/VAST/vast.shtml) was used to find structural alignment between SARS-CoV-2 Ep9 and proteins from other viral and bacterial human host pathogens. Alignment for NP from common hCoV were not further examined, as they had been included in sequence alignment analysis. The aligned sequences were sorted by the number of aligned residues as well as root-mean square deviation (RMDS). The top 50 structurally aligned proteins were then examined for structural homology in the Ep9 epitope region. Regions of proteins that aligned with the Ep9 region were selected for subsequent analysis.

Cloning

Predicted AIM epitopes were subcloned for phage display using the pM1165a phagemid vector [23] with an N-terminal FLAG-tag and a C-terminal P8 M13-bacteriophage coat protein. AIM constructs were subcloned using the Q5 site-directed mutagenesis kit (New England Biolabs,

bioRxiv preprint doi: https://doi.org/10.1101/2021.05.21.445201; this version posted June 9, 2021. The copyright holder for this preprint (which was not certified by peer review) is the author/funder. All rights reserved. No reuse allowed without permission.

Ipswich, MA) as per manufacturer's instructions. After cloning, cells were transformed into XL-1 Blue *E. coli* and spread on carbenicillin-supplemented (50 µg/ml) plates. Individual colonies were then inoculated into 5 ml cultures, and shaken overnight at 37 °C. The phagemid was isolated using the QIAprep spin miniprep kit (Qiagen, Germantown, MD) as per manufacturer's instructions. Cloned sequences were verified by Sanger sequencing (Genewiz, San Diego, CA).

Phage propagation and purification

The Ep9 homologs were expressed as N-terminal fusions to the P8 coat protein of M13 bacteriophage. Plasmids were transformed into SS320 *E. coli* and spread onto carbenicillin-supplemented (50 µg/ml) LB-agar plates before overnight incubation at 37 °C. A single colony was inoculated into a primary culture of 15 ml of 2YT supplemented with 50 µg/ml carbenicillin and 2.5 µg/ml of tetracycline, and incubated at 37 °C with shaking at 225 rpm until an optical density at 600 nm (OD_{600}) of 0.5 to 0.7 was reached. 30 µM IPTG and M13KO7 helper phage at an MOI 4.6 was added to the primary culture, and the culture was incubated for an additional 37 °C with shaking at 225 rpm for 45 min. 8 ml of the primary culture was then transferred to 300 ml of 2YT supplemented with 50 µg/ml of carbenicillin and 20 µg/ml of kanamycin. The cultures were inoculated at 30 °C with shaking at 225 rpm for around 19 h.

The phage propagation culture was centrifuged at 9632 x *g* for 10 min at 4 °C. The supernatant, containing the phage, was transferred into a separate tubes pre-aliquoted with 1/5th volume of phage precipitation buffer (20% w/v PEG-8000 and 2.5 M NaCl), and incubated on ice for 30 min. The solution, containing precipitated phage, was centrifuged for 15 min at 4 °C, and the supernatant was discarded. The precipitated phage was centrifuged a second time at 1,541 x *g* for 4 min at 4 °C, and then dissolved in 20 ml of resuspension buffer (10 mM phosphate, 137 mM NaCl, pH 7.4 - 8.0 with Tween-20 0.05%, v/v and glycerol 10% v/v). The resuspended pellet solution was divided into 1 ml aliquots, which were flash frozen with liquid nitrogen for storage in -80 °C. Prior to use in ELISA binding assays, the aliquoted phage-displayed constructs were re-

bioRxiv preprint doi: https://doi.org/10.1101/2021.05.21.445201; this version posted June 9, 2021. The copyright holder for this preprint (which was not certified by peer review) is the author/funder. All rights reserved. No reuse allowed without permission.

precipitated in 0.2 ml of phage precipitation buffer after incubation for 30 min on ice. Aliquots were centrifuged at 12298 x *g* for 20 min at 4 °C and the supernatant was discarded. The phage pellets were re-centrifuged at 1968 x *g* for 4 min at 4 °C, and then resuspended in 1 ml of 10 mM phosphate, 137 mM NaCl, pH 7.4.

Expression and Purification of eGFP fusion peptides

pET28c plasmids encoding eGFP fusions to C-terminal Ep9-FLAG, EpNeu-FLAG, EpPred-FLAG and FLAG (negative control) and N-terminal His_6 peptide epitopes, were transformed into BL21DE3 Star *E. coli* chemically competent cells. Transformants were spread on carbenicillin-supplemented (50 μg/ml) LB-agar plates and incubated at 37 °C overnight. Single colonies of each construct were selected to inoculate 25 ml LB media supplemented with carbenicillin (50 μg/ml). After incubation at 37 °C with shaking at 255 rpm overnight, 5 ml of seed cultures were used to inoculate 500 ml of LB media supplemented with carbenicillin (50 μg/ml). Expression cultures were incubated at 37 °C with shaking at 225 rpm until an OD_{600} of ~0.5 was reached. The cultures were induced with 0.5 mM IPTG and incubated at 25 °C for 18 h. The cells were pelleted by centrifugation at 9632 x *g* for 20 min and resuspended in Tris-HCl lysis buffer (20 mM Tris-HCl, 250 mM NaCl, pH 8). Cells were lysed by sonication and the insoluble fractions were pelleted by centrifugation at 24696 x *g*. The supernatant was affinity-purified using Profinity™ IMAC (BioRad, Hercules, CA) resin charged with nickel sulfate. The protein lysate was batch bound overnight to the IMAC resin and purified using gravity columns. Columns were washed with lysis buffer supplemented with 20 mM imidazole, and the elution fractions were collected from lysis buffer containing 250 mM imidazole. The elution fractions were then buffer-exchanged with lysis buffer lacking imidazole using Vivaspin® 20 Ultrafiltration Units (Sartorius, Goettingen, Germany) with a molecular weight cutoff of 10 kDa. The final buffer imidazole

bioRxiv preprint doi: https://doi.org/10.1101/2021.05.21.445201; this version posted June 9, 2021. The copyright holder for this preprint (which was not certified by peer review) is the author/funder. All rights reserved. No reuse allowed without permission.

concentrations were calculated to be ~0.1 mM. Purified and buffer-exchanged protein fractions were then visualized using 10% SDS-PAGE with Coomassie dye staining.

Patient Sample Collection

Samples were collected as previously described [9]. Briefly, the UC Irvine Experimental Tissue Resource (ETR) operates under a blanket IRB protocol (UCI #2012-8716) which enables sample collection in excess of requirements for clinical diagnosis, and allows distribution to investigators. Plasma was collected from daily blood draws of COVID(+) patients, initially confirmed with pharyngeal swabs. After immediate centrifugation, plasma from heparin-anticoagulated blood was stored for 3-4 days at 4 °C prior to its release for research use. Personal health information was omitted and unique de-identifier codes were assigned to patients to comply with the Non-Human Subjects Determination exemption from the UCI IRB. At the research facility, SARS-CoV-2 virus in plasma samples was inactivated through treatment by incubation in a 56 °C water bath for 30 min[24] prior to storage at -80 °C.

Phage ELISAs

As described in previous reports [9], pooled plasma from five αEp9(+) patients, five αEp9(-) patients, or healthy patients (Sigma-Aldrich, Saint Louis, MO) were separately prepared in coating buffer (50 mM Na_2CO_3, pH 9.6); the plasma was diluted 100-fold during this step. Plasma samples were then immobilized in 96 well microtiter plates by shaking the plasma solutions at 150 rpm at room temperature (RT) for 30 min. After aspiration and washing by plate washer (BioTek, Winooski, VT), each well was blocked with 100 µL of ChonBlock Blocking Buffer (CBB) (Chondrex, Inc., Woodinville, WA) for 30 mins, shaking at 150 rpm at RT. Wells were subsequently washed three times with PBS-T (0.05% v/v Tween-20 in PBS). Next, 1 nM phage-displayed candidate “original” epitopes and controls prepared in CBB was incubated in microtiter wells for 1 h at RT with shaking at 150 rpm. Unbound phage were aspirated and removed using

bioRxiv preprint doi: https://doi.org/10.1101/2021.05.21.445201; this version posted June 9, 2021. The copyright holder for this preprint (which was not certified by peer review) is the author/funder. All rights reserved. No reuse allowed without permission.

three washes with PBS-T. The peroxidase-conjugated detection antibody, αM13-HRP (Creative Diagnostics, Shirley, NY), was diluted 1000-fold in Chonblock Secondary Antibody Dilution (Chondrex, Inc., Woodinville, WA) buffer; 100 µl of this solution was added to each well before incubation for 30 min at RT with shaking at 150 rpm. Following aspiration and three washes (100 µl each), 1-Step Ultra TMB-ELISA Substrate Solution (ThermoScientific, Carlsbad, CA) was added (100 µl per well). Absorbance of TMB substrate was measured twice at 652 nm by UV-Vis plate reader (BioTek Winooski, VT) after 5 and 15 min of incubation. The experiment was repeated three times using plasma from different αEp9(+) and αEp9(-) patients for each experiments, using a total of 15 patients for each group. Each experiment was conducted in technical duplicate.

αEp9 IgG and IgM ELISA

Plasma from 34 patients, previously tested for the presence of αEp9 Abs using phage ELISAs[9], were used to test levels of αEp9 IgGs and IgMs. 2 µM eGFP-Ep9 or eGFP-FLAG in PBS pH 8.0 were immobilized onto 96 well microtiter plates via overnight incubation with shaking at 150 rpm at 4 °C. Excess protein was aspirated and removed with three consecutive PBS-T washes. Wells were blocked by adding CBB (100 µl) before incubation at 30 min at RT with shaking at 150 rpm. Next, αEp9(+) patient plasma, diluted 1:100 in CBB (100 µl), was added to duplicate wells before incubation at RT for 1 h with shaking at 150 rpm. The solutions were discarded and sample wells were washed with PBS-T three times. αEp9 Abs binding to the potential epitopes was detected using horse radish peroxidase (HRP) conjugated αHuman Fc IgG (Thermo Fisher Scientific, Waltham MA) or αIgM µ-chain specific (Millipore Sigma, Temecula, CA) Abs diluted 1:5000 in ChonBlock Sample Antibody Dilution buffer. 100 µl of detection Abs were added to each sample well, and incubated for 30 min at RT with shaking at 150 rpm. Sample wells were aspirated and washed three times in PBS-T, and the binding signal was detected after addition of TMB substrate (100 µl per well).

bioRxiv preprint doi: https://doi.org/10.1101/2021.05.21.445201; this version posted June 9, 2021. The copyright holder for this preprint (which was not certified by peer review) is the author/funder. All rights reserved. No reuse allowed without permission.

Bivalent Abs binding ELISA

eGFP-Ep9 or eGFP-FLAG was serially diluted (120 nM, 40 nM, 13 nM and 4 nM) in PBS pH 8.0, and added to the appropriate wells in 96 well microtiter plates, followed by shaking overnight at 150 rpm at 4 °C. Excess unbound protein was removed, and the plate was washed three times in PBS-T. Wells were then blocked in CBB and incubated for 30 min at RT. After blocking, pooled plasma (100 µl per well) from either five αEp9(+) patients, or five non-αEp9, αNP(+) patients, or healthy individuals was added to the appropriate wells. Plasma from pooled patients was diluted 100-fold in CBB. As a positive control αFLAG Ab was used as a 1:2000 dilution in CBB. Samples were incubated for 1 h at RT with 150 rpm shaking. The solution was removed by aspiration, and the plate and washed three times with PBS-T. Then 1 nM EpNeu displaying phage or the phage negative control with no epitopes displayed was diluted in CBB. 100 µl phage solution was added to microtiter wells and incubated for 30 min at RT with shaking at 150 rpm. After aspirating and washing off unbound phage, binding of phage-displayed EpNeu to plasma αEp9 Abs was visualized using αM13-HRP Ab diluted 1:10,000 in ChonBlock Sample Antibody Dilution buffer. Samples were incubated for 30 min at RT with 150 rpm shaking, and unbound Abs were removed through washing with PBS-T three times before addition of TMB substrate (100 µl). Experiments were conducted in technical triplicates and repeated three times with different αEp(+) and αEp(-) patient samples.

Dose-dependent ELISA

Wells of microtiter plates were coated with serially diluted concentration of eGFP-Ep9, EpNeu and EpPred or eGFP-FLAG, and incubated overnight at 4 °C before blocking as described above. Next, pooled plasma (100 µl per well) from either five αEp9(+) patients, or five αEp9(-) patients, or healthy individuals at 1:100 total plasma dilution in CBB was added to the appropriate wells. Samples were incubated for 1 h at RT with shaking at 150 rpm. After incubation, unbound solution was removed, and the plates were washed three times with PBS-T. αEp9 IgG levels were

bioRxiv preprint doi: https://doi.org/10.1101/2021.05.21.445201; this version posted June 9, 2021. The copyright holder for this preprint (which was not certified by peer review) is the author/funder. All rights reserved. No reuse allowed without permission.

detected by adding αFc IgG-HRP diluted 1:5000 in ChonBlock Sample Dilution buffer, followed by incubation for 30 min at RT with shaking at 150 rpm, followed by addition of TMB substrate (100 µl per well). Experiments were conducted in technical triplicates and repeated three times with different αEp(+) and αEp(-) patient samples.

Linear B-cell Epitope Prediction

Linear epitopes from the Influenza A/Para/128982-IEC/2014(H3N2) neuraminidase protein were predicted using the partial sequence with Accession AIX95025.1 from the National Center for Biotechnology Information's GenBank and the linear B-cell epitope prediction tool, Bepipred 2.0[13] (http://www.cbs.dtu.dk/services/BepiPred-2.0/). The prediction thresholds were set to 0.5. The specificity and sensitivity of epitope prediction at this threshold is 0.572 and 0.586, respectively.

Structure-based B-cell epitope prediction

The structure of Influenza A/Para/128982-IEC/2014(H3N2) neuraminidase protein was modelled using Swiss-Model[21] (https://swissmodel.expasy.org/interactive). Using the ProMod3 3.2.0 tool[15], a structural model was generated based on the crystal structure (2.35Å, PDB 4GZS 1.A) of a homologous H3N2 neuraminidase with 96.39% sequence identity. Modelling methods and quality assessments are further detailed in the report below.

The structural model of Influenza A/Para/128982-IEC/2014(H3N2) neuraminidase was used to predict structure-based epitopes. Using the *in silico* online platform Discotope 2.0[16] (http://www.cbs.dtu.dk/services/DiscoTope-2.0/), structure-based epitope propensity scores were calculated to predict likely B-cell epitope residues. The score of -3.7 was set as the threshold for epitope prediction, which estimates a specificity and sensitivity of 0.75 and 0.47, respectively (Figure S4)

bioRxiv preprint doi: https://doi.org/10.1101/2021.05.21.445201; this version posted June 9, 2021. The copyright holder for this preprint (which was not certified by peer review) is the author/funder. All rights reserved. No reuse allowed without permission.

Statistical Analysis

The ELISA data were analyzed in GraphPad Prism 9 (https://www.graphpad.com). Since the ELISA assays of 21 potential AIM epitopes were conducted over several microtiter plates for repeated experiments, the raw absorbance values for every patient sample were normalized and represented as the ratio of phage negative control to the signal. For heatmaps, two-way Analysis of variance (ANOVA) with a Tukey adjustment for multiple comparisons tests were conducted for the entire dataset of epitopes. For column comparisons of two groups, for example IgM levels and IgG levels in the αEp(+) patients, unpaired, two-tailed, parametric t-tests were applied. Additionally, for column comparisons between more than two groups, for example IgM or IgG levels groups by weeks PSO, One-way ANOVA with a Tukey adjustment for multiple comparisons tests were used. Where indicated, an ANOVA with a Dunnett's adjustment were performed to compare results to healthy Abs interactions to αEp9(+) patient results. Graphs represent SD error bars for technical replicates, defined as replicates of the same conditions in multiple wells of the same plate. Whereas error bars are shown as SEM when an experiment is repeated with different patient sample sets. Correlations between Ep9 and EpNeu levels in patients were determined by plotting normalized values on an XY graph and performing a linear Pearson's correlation coefficient test, where a *r* coefficient between 1.0-0.7 were considered strong correlations, values between 0.7 and 0.5 were considered a moderate correlation, and values below 0.5 were considered a weak correlation[25]. The significance of the correlation was evaluated based on p-value <0.05.

bioRxiv preprint doi: https://doi.org/10.1101/2021.05.21.445201; this version posted June 9, 2021. The copyright holder for this preprint (which was not certified by peer review) is the author/funder. All rights reserved. No reuse allowed without permission.

456

BIOZENTRUM
University of Basel
The Center for Molecular Life Sciences

SWISS-MODEL Homology Modelling Report

Model Building Report

This document lists the results for the homology modelling project "Untitled Project" submitted to SWISS-MODEL workspace on March 30, 2021, 10:35 a.m..The submitted primary amino acid sequence is given in Table T1.

If you use any results in your research, please cite the relevant publications:

- Waterhouse, A., Bertoni, M., Bienert, S., Studer, G., Tauriello, G., Gumienny, R., Heer, F.T., de Beer, T.A.P., Rempfer, C., Bordoli, L., Lepore, R., Schwede, T. SWISS-MODEL: homology modelling of protein structures and complexes. Nucleic Acids Res. 46(W1), W296-W303 (2018). doi>
- Bienert, S., Waterhouse, A., de Beer, T.A.P., Tauriello, G., Studer, G., Bordoli, L., Schwede, T. The SWISS-MODEL Repository - new features and functionality. Nucleic Acids Res. 45, D313-D319 (2017). doi>
- Studer, G., Tauriello, G., Bienert, S., Biasini, M., Johner, N., Schwede, T. ProMod3 - A versatile homology modelling toolbox. PLOS Comp. Biol. 17(1), e1008667 (2021). doi>
- Studer, G., Rempfer, C., Waterhouse, A.M., Gumienny, G., Haas, J., Schwede, T. QMEANDisCo - distance constraints applied on model quality estimation. Bioinformatics 36, 1765-1771 (2020). doi>
- Bertoni, M., Kiefer, F., Biasini, M., Bordoli, L., Schwede, T. Modeling protein quaternary structure of homo- and hetero-oligomers beyond binary interactions by homology. Scientific Reports 7 (2017). doi>

Results

The SWISS-MODEL template library (SMTL version 2021-03-25, PDB release 2021-03-19) was searched with BLAST (Camacho et al.) and HHblits (Steinegger et al.) for evolutionary related structures matching the target sequence in Table T1. For details on the template search, see Materials and Methods. Overall 189 templates were found (Table T2).

Models

The following model was built (see Materials and Methods "Model Building"):

Model #01	File	Built with	Oligo-State	Ligands	GMQE	QMEAN
	PDB	ProMod3 3.2.0	homo-tetramer (matching prediction)	4 x CA: CALCIUM ION; 1 x NAG: 2-acetamido-2-deoxy-beta-D-glucopyranose; 1 x NAG-FUC: alpha-L-fucopyranose-(1-6)-2-acetamido-2-deoxy-beta-D-glucopyranose;	0.95	-1.40

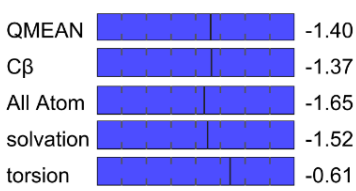

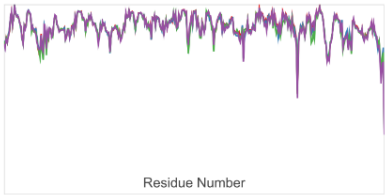

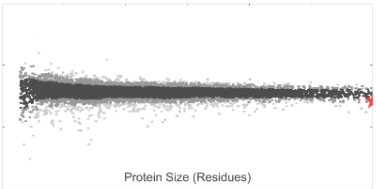

Template	Seq Identity	Oligo-state	QSQE	Found by	Method	Resolution	Seq Similarity	Range	Coverage	Description
4gzs.1.A	96.39	homo-tetramer	1.00	HHblits	X-ray	2.35Å	0.62	1 - 360	1.00	Neuraminidase

Included Ligands

Ligand	Description
4 x CA	CALCIUM ION
1 x NAG	2-acetamido-2-deoxy-beta-D-glucopyranose
1 x NAG-FUC	alpha-L-fucopyranose-(1-6)-2-acetamido-2-deoxy-beta-D-glucopyranose

bioRxiv preprint doi: https://doi.org/10.1101/2021.05.21.445201; this version posted June 9, 2021. The copyright holder for this preprint (which was not certified by peer review) is the author/funder. All rights reserved. No reuse allowed without permission.

Excluded ligands

Ligand Name.Number	Reason for Exclusion	Description
CA.16	Not in contact with model.	CALCIUM ION
EPE.10	Not biologically relevant.	4-(2-HYDROXYETHYL)-1-PIPERAZINE ETHANESULFONIC ACID
EPE.13	Not biologically relevant.	4-(2-HYDROXYETHYL)-1-PIPERAZINE ETHANESULFONIC ACID
EPE.18	Not biologically relevant.	4-(2-HYDROXYETHYL)-1-PIPERAZINE ETHANESULFONIC ACID
EPE.22	Not biologically relevant.	4-(2-HYDROXYETHYL)-1-PIPERAZINE ETHANESULFONIC ACID
NAG.11	Clashing with protein.	2-acetamido-2-deoxy-beta-D-glucopyranose
NAG.14	Clashing with protein.	2-acetamido-2-deoxy-beta-D-glucopyranose
NAG.15	Clashing with protein.	2-acetamido-2-deoxy-beta-D-glucopyranose
NAG.19	Clashing with protein.	2-acetamido-2-deoxy-beta-D-glucopyranose
NAG.20	Not in contact with model.	2-acetamido-2-deoxy-beta-D-glucopyranose
NAG.24	Clashing with protein.	2-acetamido-2-deoxy-beta-D-glucopyranose
NAG-FUC.2	Clashing with protein.	alpha-L-fucopyranose-(1-6)-2-acetamido-2-deoxy-beta-D-glucopyranose
NAG-FUC.4	Clashing with protein.	alpha-L-fucopyranose-(1-6)-2-acetamido-2-deoxy-beta-D-glucopyranose
NAG-NAG.8	Not in contact with model.	2-acetamido-2-deoxy-beta-D-glucopyranose-(1-4)-2-acetamido-2-deoxy-beta-D-glucopyranose
NAG-NAG-BMA-MAN-MAN.1	Clashing with protein.	alpha-D-mannopyranose-(1-3)-[alpha-D-mannopyranose-(1-6)]beta-D-mannopyranose-(1-4)-2-acetamido-2-deoxy-beta-D-glucopyranose-(1-4)-2-acetamido-2-deoxy-beta-D-glucopyranose
NAG-NAG-BMA-MAN-MAN.3	Clashing with protein.	alpha-D-mannopyranose-(1-3)-[alpha-D-mannopyranose-(1-6)]beta-D-mannopyranose-(1-4)-2-acetamido-2-deoxy-beta-D-glucopyranose-(1-4)-2-acetamido-2-deoxy-beta-D-glucopyranose
NAG-NAG-BMA-MAN-MAN.5	Clashing with protein.	alpha-D-mannopyranose-(1-3)-[alpha-D-mannopyranose-(1-6)]beta-D-mannopyranose-(1-4)-2-acetamido-2-deoxy-beta-D-glucopyranose-(1-4)-2-acetamido-2-deoxy-beta-D-glucopyranose
NAG-NAG-BMA-MAN-MAN.7	Not biologically relevant.	alpha-D-mannopyranose-(1-3)-[alpha-D-mannopyranose-(1-6)]beta-D-mannopyranose-(1-4)-2-acetamido-2-deoxy-beta-D-glucopyranose-(1-4)-2-acetamido-2-deoxy-beta-D-glucopyranose

```
Target     AGGDIWVTREPYVSCDPDKGNQFALGQGTTLSKGHSNNTVRDRTPYRTLLMNELGVPFHLGTKQVCIAWSSSSCHDGKAW
4gzs.1.A   AGGDIWVTREPYVSCDPDKCYQFALGQGTTLNNVHSNNTVRGRTPYRTLLMNELGVPFHLGTKQVCIAWSSSSCHDGKAW

Target     LHVCITGDDKNATASFIYNGRLVDSVVSWSKEVLRTQESECVCINGTCTVVMTDGSASGKADTKILFIEEGKIVHTSTLS
4gzs.1.A   LHVCITGDDKNATASFIYNGRLVDSVVSWSKEILRTQESECVCINGTCTVVMTDGSASGKADTKILFIEEGKIVHTSTLS

Target     GSAQHVEECSCYPRYPGVRCVCRDNWKGSNRPIVDINIKDHSIVSSYVCSGLVGDTPRKNDSSSSGHCLNPNNEEGGHGV
4gzs.1.A   GSAQHVEECSCYPRYPGVRCVCRDNWKGSNRPIVDINIKDHSIVSSYVCSGLVGDTPRKNDSSSSSHCLDPNNEEGGHGV

Target     KGWAFDDGNDVWMGRTINETSRLGYETFKVIEGWSNPKSKLQINRQVIVDRGDRSGYSGIFSVEGKSCINRCFYVELIRG
4gzs.1.A   KGWAFDDGNDVWMGRTINETSRLGYETFKVIEGWSNPKSKLQINRQVIVDRGNRSGYSGIFSVEGKSCINRCFYVELIRG

Target     RKEETEVLWTSNSILLFCGTSGTYGTGSWPDAADLNLMPI
4gzs.1.A   RKEETEVLWTSNSIVVFCGTSGTYGTGSWPDGADLNLMPI
```

bioRxiv preprint doi: https://doi.org/10.1101/2021.05.21.445201; this version posted June 9, 2021. The copyright holder for this preprint (which was not certified by peer review) is the author/funder. All rights reserved. No reuse allowed without permission.

```
Target    AGGDIWVTREPYVSCDPDKGNQFALGQGTTLSKGHSNNTVRDRTPYRTLLMNELGVPFHLGTKQVCIAWSSSSCHDGKAW
4gzs.1.B  AGGDIWVTREPYVSCDPDKCYQFALGQGTTLNNVHSNNTVRGRTPYRTLLMNELGVPFHLGTKQVCIAWSSSSCHDGKAW

Target    LHVCITGDDKNATASFIYNGRLVDSVVSWSKEVLRTQESECVCINGTCTVVMTDGSASGKADTKILFIEEGKIVHTSTLS
4gzs.1.B  LHVCITGDDKNATASFIYNGRLVDSVVSWSKEILRTQESECVCINGTCTVVMTDGSASGKADTKILFIEEGKIVHTSTLS

Target    GSAQHVEECSCYPRYPGVRCVCRDNWKGSNRPIVDINIKDHSIVSSYVCSGLVGDTPRKNDSSSSGHCLNPNNEEGGHGV
4gzs.1.B  GSAQHVEECSCYPRYPGVRCVCRDNWKGSNRPIVDINIKDHSIVSSYVCSGLVGDTPRKNDSSSSSHCLDPNNEEGGHGV

Target    KGWAFDDGNDVWMGRTINETSRLGYETFKVIEGWSNPKSKLQINRQVIVDRGDRSGYSGIFSVEGKSCINRCFYVELIRG
4gzs.1.B  KGWAFDDGNDVWMGRTINETSRLGYETFKVIEGWSNPKSKLQINRQVIVDRGNRSGYSGIFSVEGKSCINRCFYVELIRG

Target    RKEETEVLWTSNSILLFCGTSGTYGTGSWPDAADLNLMPI
4gzs.1.B  RKEETEVLWTSNSIVVFCGTSGTYGTGSWPDGADLNLMPI


Target    AGGDIWVTREPYVSCDPDKGNQFALGQGTTLSKGHSNNTVRDRTPYRTLLMNELGVPFHLGTKQVCIAWSSSSCHDGKAW
4gzs.1.C  AGGDIWVTREPYVSCDPDKCYQFALGQGTTLNNVHSNNTVRGRTPYRTLLMNELGVPFHLGTKQVCIAWSSSSCHDGKAW

Target    LHVCITGDDKNATASFIYNGRLVDSVVSWSKEVLRTQESECVCINGTCTVVMTDGSASGKADTKILFIEEGKIVHTSTLS
4gzs.1.C  LHVCITGDDKNATASFIYNGRLVDSVVSWSKEILRTQESECVCINGTCTVVMTDGSASGKADTKILFIEEGKIVHTSTLS

Target    GSAQHVEECSCYPRYPGVRCVCRDNWKGSNRPIVDINIKDHSIVSSYVCSGLVGDTPRKNDSSSSGHCLNPNNEEGGHGV
4gzs.1.C  GSAQHVEECSCYPRYPGVRCVCRDNWKGSNRPIVDINIKDHSIVSSYVCSGLVGDTPRKNDSSSSSHCLDPNNEEGGHGV

Target    KGWAFDDGNDVWMGRTINETSRLGYETFKVIEGWSNPKSKLQINRQVIVDRGDRSGYSGIFSVEGKSCINRCFYVELIRG
4gzs.1.C  KGWAFDDGNDVWMGRTINETSRLGYETFKVIEGWSNPKSKLQINRQVIVDRGNRSGYSGIFSVEGKSCINRCFYVELIRG

Target    RKEETEVLWTSNSILLFCGTSGTYGTGSWPDAADLNLMPI
4gzs.1.C  RKEETEVLWTSNSIVVFCGTSGTYGTGSWPDGADLNLMPI


Target    AGGDIWVTREPYVSCDPDKGNQFALGQGTTLSKGHSNNTVRDRTPYRTLLMNELGVPFHLGTKQVCIAWSSSSCHDGKAW
4gzs.1.D  AGGDIWVTREPYVSCDPDKCYQFALGQGTTLNNVHSNNTVRGRTPYRTLLMNELGVPFHLGTKQVCIAWSSSSCHDGKAW

Target    LHVCITGDDKNATASFIYNGRLVDSVVSWSKEVLRTQESECVCINGTCTVVMTDGSASGKADTKILFIEEGKIVHTSTLS
4gzs.1.D  LHVCITGDDKNATASFIYNGRLVDSVVSWSKEILRTQESECVCINGTCTVVMTDGSASGKADTKILFIEEGKIVHTSTLS

Target    GSAQHVEECSCYPRYPGVRCVCRDNWKGSNRPIVDINIKDHSIVSSYVCSGLVGDTPRKNDSSSSGHCLNPNNEEGGHGV
4gzs.1.D  GSAQHVEECSCYPRYPGVRCVCRDNWKGSNRPIVDINIKDHSIVSSYVCSGLVGDTPRKNDSSSSSHCLDPNNEEGGHGV

Target    KGWAFDDGNDVWMGRTINETSRLGYETFKVIEGWSNPKSKLQINRQVIVDRGDRSGYSGIFSVEGKSCINRCFYVELIRG
4gzs.1.D  KGWAFDDGNDVWMGRTINETSRLGYETFKVIEGWSNPKSKLQINRQVIVDRGNRSGYSGIFSVEGKSCINRCFYVELIRG

Target    RKEETEVLWTSNSILLFCGTSGTYGTGSWPDAADLNLMPI
4gzs.1.D  RKEETEVLWTSNSIVVFCGTSGTYGTGSWPDGADLNLMPI
```

Materials and Methods

Template Search

Template search with BLAST and HHblits has been performed against the SWISS-MODEL template library (SMTL, last update: 2021-03-25, last included PDB release: 2021-03-19).

The target sequence was searched with BLAST against the primary amino acid sequence contained in the SMTL. A total of 103 templates were found.

bioRxiv preprint doi: https://doi.org/10.1101/2021.05.21.445201; this version posted June 9, 2021. The copyright holder for this preprint (which was not certified by peer review) is the author/funder. All rights reserved. No reuse allowed without permission.

An initial HHblits profile has been built using the procedure outlined in (Steinegger et al.), followed by 1 iteration of HHblits against Uniclust30 (Mirdita, von den Driesch et al.). The obtained profile has then be searched against all profiles of the SMTL. A total of 104 templates were found.

Template Selection

For each identified template, the template's quality has been predicted from features of the target-template alignment. The templates with the highest quality have then been selected for model building.

Model Building

Models are built based on the target-template alignment using ProMod3 (Studer et al.). Coordinates which are conserved between the target and the template are copied from the template to the model. Insertions and deletions are remodelled using a fragment library. Side chains are then rebuilt. Finally, the geometry of the resulting model is regularized by using a force field.

Model Quality Estimation

The global and per-residue model quality has been assessed using the QMEAN scoring function (Studer et al.).

Ligand Modelling

Ligands present in the template structure are transferred by homology to the model when the following criteria are met: (a) The ligands are annotated as biologically relevant in the template library, (b) the ligand is in contact with the model, (c) the ligand is not clashing with the protein, (d) the residues in contact with the ligand are conserved between the target and the template. If any of these four criteria is not satisfied, a certain ligand will not be included in the model. The model summary includes information on why and which ligand has not been included.

Oligomeric State Conservation

The quaternary structure annotation of the template is used to model the target sequence in its oligomeric form. The method (Bertoni et al.) is based on a supervised machine learning algorithm, Support Vector Machines (SVM), which combines interface conservation, structural clustering, and other template features to provide a quaternary structure quality estimate (QSQE). The QSQE score is a number between 0 and 1, reflecting the expected accuracy of the interchain contacts for a model built based a given alignment and template. Higher numbers indicate higher reliability. This complements the GMQE score which estimates the accuracy of the tertiary structure of the resulting model.

References

- **BLAST**
  Camacho, C., Coulouris, G., Avagyan, V., Ma, N., Papadopoulos, J., Bealer, K., Madden, T.L. BLAST+: architecture and applications. BMC Bioinformatics 10, 421-430 (2009). doi>
- **HHblits**
  Steinegger, M., Meier, M., Mirdita, M., Vöhringer, H., Haunsberger, S. J., Söding, J. HH-suite3 for fast remote homology detection and deep protein annotation. BMC Bioinformatics 20, 473 (2019). doi>
- **Uniclust30**
  Mirdita, M., von den Driesch, L., Galiez, C., Martin, M.J., Söding, J., Steinegger, M. Uniclust databases of clustered and deeply annotated protein sequences and alignments. Nucleic Acids Research 45, D170–D176 (2016). doi>

Table T1:

Primary amino acid sequence for which templates were searched and models were built.

```
AGGDIWVTREPYVSCDPDKGNQFALGQGTTLSKGHSNNTVRDRTPYRTLLMNELGVPFHLGTKQVCIAWSSSSCHDGKAWLHVCITGDDKNATASFIYNG
RLVDSVVSWSKEVLRTQESECVCINGTCTVVMTDGSASGKADTKILFIEEGKIVHTSTLSGSAQHVEECSCYPRYPGVRCVCRDNWKGSNRPIVDINIKD
HSIVSSYVCSGLVGDTPRKNDSSSSGHCLNPNNEEGGHGVKGWAFDDGNDVWMGRTINETSRLGYETFKVIEGWSNPKSKLQINRQVIVDRGDRSGYSGI
FSVEGKSCINRCFYVELIRGRKEETEVLWTSNSILLFCGTSGTYGTGSWPDAADLNLMPI
```

Table T2:

Template	Seq Identity	Oligo-state	QSQE	Found by	Method	Resolution	Seq Similarity	Coverage	Description
4gzs.1.A	96.39	homo-tetramer	1.00	HHblits	X-ray	2.35Å	0.62	1.00	Neuraminidase
4gzo.1.A	96.67	homo-tetramer	1.00	HHblits	X-ray	2.60Å	0.62	1.00	neuraminidase

bioRxiv preprint doi: https://doi.org/10.1101/2021.05.21.445201; this version posted June 9, 2021. The copyright holder for this preprint (which was not certified by peer review) is the author/funder. All rights reserved. No reuse allowed without permission.

Template	Seq Identity	Oligo-state	QSQE	Found by	Method	Resolution	Seq Similarity	Coverage	Description
3tia.1.A	82.78	homo-tetramer	1.00	HHblits	X-ray	1.80Å	0.57	1.00	Neuraminidase
4k1j.1.A	82.78	homo-tetramer	1.00	HHblits	X-ray	2.20Å	0.57	1.00	Neuraminidase
4h52.1.A	82.78	homo-tetramer	1.00	HHblits	X-ray	1.80Å	0.57	1.00	Neuraminidase
5huk.1.A	79.72	homo-tetramer	1.00	HHblits	X-ray	2.45Å	0.57	1.00	Neuraminidase
6n4d.1.A	79.17	homo-tetramer	1.00	HHblits	X-ray	1.80Å	0.56	1.00	Neuraminidase
2bat.1.A	83.06	homo-tetramer	1.00	HHblits	X-ray	2.00Å	0.57	1.00	NEURAMINIDASE N2
1ivg.1.A	82.78	homo-tetramer	1.00	HHblits	X-ray	1.90Å	0.57	1.00	INFLUENZA A SUBTYPE N2 NEURAMINIDASE
1ive.1.A	82.78	homo-tetramer	1.00	HHblits	X-ray	2.40Å	0.57	1.00	INFLUENZA A SUBTYPE N2 NEURAMINIDASE
1inh.1.A	82.78	homo-tetramer	1.00	HHblits	X-ray	2.40Å	0.57	1.00	INFLUENZA A SUBTYPE N2 NEURAMINIDASE
1ing.1.A	82.78	homo-tetramer	1.00	HHblits	X-ray	2.40Å	0.57	1.00	INFLUENZA A SUBTYPE N2 NEURAMINIDASE
6br5.1.A	95.83	monomer	-	HHblits	X-ray	2.04Å	0.62	1.00	Neuraminidase
2aep.1.A	90.56	homo-tetramer	1.00	HHblits	X-ray	2.10Å	0.60	1.00	neuraminidase
6n6b.1.A	89.17	homo-tetramer	1.00	HHblits	X-ray	2.30Å	0.60	1.00	Neuraminidase
4mwx.1.B	47.62	homo-tetramer	0.86	HHblits	X-ray	1.80Å	0.44	0.99	Neuraminidase
4mwj.1.A	47.90	homo-tetramer	0.85	HHblits	X-ray	1.80Å	0.44	0.99	Neuraminidase
5nz4.1.A	46.05	homo-tetramer	0.88	HHblits	X-ray	1.36Å	0.43	0.98	neuraminidase
2b8h.1.A	47.62	homo-tetramer	0.85	HHblits	X-ray	2.20Å	0.44	0.99	Neuraminidase
4m3m.1.A	44.94	homo-tetramer	0.87	HHblits	X-ray	2.10Å	0.43	0.99	Neuraminidase
5l14.1.A	47.90	homo-tetramer	0.84	HHblits	X-ray	1.90Å	0.44	0.99	Neuraminidase
4mwj.1.A	49.72	homo-tetramer	0.84	BLAST	X-ray	1.80Å	0.45	0.98	Neuraminidase
2b8h.1.A	49.43	homo-tetramer	0.84	BLAST	X-ray	2.20Å	0.45	0.98	Neuraminidase
1nna.1.D	49.15	homo-tetramer	0.84	BLAST	X-ray	2.50Å	0.44	0.98	NEURAMINIDASE
4mju.1.A	45.51	homo-tetramer	0.84	HHblits	X-ray	2.35Å	0.43	0.99	Neuraminidase
4nn9.1.A	49.15	homo-tetramer	0.83	BLAST	X-ray	2.30Å	0.44	0.98	NEURAMINIDASE N9
1mwe.1.C	49.15	homo-tetramer	0.83	BLAST	X-ray	1.70Å	0.44	0.98	NEURAMINIDASE
6pzw.1.A	47.90	homo-tetramer	0.87	HHblits	EM	NA	0.44	0.99	Neuraminidase
6pze.1.A	47.90	homo-tetramer	0.83	HHblits	X-ray	2.30Å	0.44	0.99	Neuraminidase
6pze.1.A	49.72	homo-tetramer	0.83	BLAST	X-ray	2.30Å	0.45	0.98	Neuraminidase

bioRxiv preprint doi: https://doi.org/10.1101/2021.05.21.445201; this version posted June 9, 2021. The copyright holder for this preprint (which was not certified by peer review) is the author/funder. All rights reserved. No reuse allowed without permission.

464

Template	Seq Identity	Oligo-state	QSQE	Found by	Method	Resolution	Seq Similarity	Coverage	Description
6pzf.1.A	47.90	homo-tetramer	0.84	HHblits	X-ray	2.80Å	0.44	0.99	Neuraminidase
1nca.2.C	49.15	homo-tetramer	0.84	BLAST	X-ray	2.50Å	0.44	0.98	INFLUENZA A SUBTYPE N9 NEURAMINIDASE
1ncd.1.A	47.90	homo-tetramer	0.84	HHblits	X-ray	2.90Å	0.44	0.99	INFLUENZA A SUBTYPE N9 NEURAMINIDASE
1nmb.1.A	47.90	homo-tetramer	0.81	HHblits	X-ray	2.20Å	0.44	0.99	N9 NEURAMINIDASE
4d8s.1.A	45.79	homo-tetramer	0.88	HHblits	X-ray	2.40Å	0.43	0.99	Neuraminidase
4gb1.1.A	45.79	homo-tetramer	0.85	HHblits	X-ray	2.62Å	0.43	0.99	Neuraminidase
4b7q.1.A	46.18	homo-tetramer	0.85	HHblits	X-ray	2.73Å	0.43	0.98	NEURAMINIDASE
3o9j.1.A	45.92	homo-tetramer	0.84	HHblits	X-ray	2.00Å	0.43	0.99	Neuraminidase
4mjv.1.A	45.79	homo-tetramer	0.83	HHblits	X-ray	2.65Å	0.43	0.99	Neuraminidase
2ht7.1.A	45.51	homo-tetramer	0.81	HHblits	X-ray	2.60Å	0.43	0.99	Neuraminidase
4ks5.1.A	44.94	homo-tetramer	0.77	HHblits	X-ray	2.70Å	0.43	0.99	Neuraminidase
6crd.1.D	49.15	homo-tetramer	0.75	BLAST	X-ray	2.57Å	0.44	0.98	Tetrabrachion,Neuraminidase
6crd.1.B	49.15	homo-tetramer	0.75	BLAST	X-ray	2.57Å	0.44	0.98	Tetrabrachion,Neuraminidase
6crd.1.C	49.15	homo-tetramer	0.75	BLAST	X-ray	2.57Å	0.44	0.98	Tetrabrachion,Neuraminidase
1ncc.1.A	49.15	homo-tetramer	0.86	BLAST	X-ray	2.50Å	0.44	0.98	INFLUENZA A SUBTYPE N9 NEURAMINIDASE
1ncd.1.A	49.43	homo-tetramer	0.83	BLAST	X-ray	2.90Å	0.45	0.98	INFLUENZA A SUBTYPE N9 NEURAMINIDASE
1nmb.1.A	49.43	homo-tetramer	0.81	BLAST	X-ray	2.20Å	0.45	0.98	N9 NEURAMINIDASE
6lxk.1.A	48.13	homo-tetramer	0.84	BLAST	X-ray	3.61Å	0.44	0.96	Neuraminidase
1nma.1.A	47.62	homo-tetramer	0.68	HHblits	X-ray	3.00Å	0.44	0.99	N9 NEURAMINIDASE
1nma.1.A	49.43	homo-tetramer	0.65	BLAST	X-ray	3.00Å	0.45	0.98	N9 NEURAMINIDASE

The table above shows the top 50 filtered templates. A further 83 templates were found which were considered to be less suitable for modelling than the filtered list.
1a4g.1.A, 1b9v.1.D, 1inf.1.A, 1iny.1.A, 1l7g.1.A, 1mwe.1.C, 1nca.2.C, 1ncb.1.A, 1ncc.1.A, 1nna.1.D, 1vcj.1.A, 2ht7.1.A, 2htv.1.A, 2hu0.1.A, 2qwd.1.A, 3b7e.1.A, 3cl0.1.A, 3cl2.1.A, 3cye.1.A, 3f14.1.A, 3k36.1.A, 3k38.1.A, 3nn9.1.A, 3o9j.1.A, 3sal.1.A, 4b7m.1.C, 4b7q.1.A, 4b7r.1.A, 4cpl.1.A, 4cpo.1.A, 4d8s.1.A, 4fvk.1.A, 4gb1.1.A, 4gdi.1.A, 4gdi.1.B, 4gdj.1.A, 4gez.1.A, 4h53.1.A, 4h53.1.D, 4hzv.1.A, 4hzy.1.A, 4hzz.1.A, 4k3y.1.A, 4k3y.1.C, 4ks5.1.A, 4m3m.1.A, 4mc7.1.A, 4mju.1.A, 4mjv.1.A, 4mwx.1.B, 4nn9.1.A, 4qn3.1.A, 4qn4.1.A, 4qnp.1.A, 4wa5.1.D, 5hug.1.A, 5hum.1.A, 5hun.1.A, 5l14.1.A, 5nn9.1.A, 5nwe.1.A, 5nz4.1.A, 5nze.1.A, 5nzf.1.A, 5nzn.1.A, 6crd.1.A, 6crd.1.B, 6crd.1.C, 6crd.1.D, 6d96.1.A, 6g01.2.D, 6hfy.1.D, 6hp0.1.C, 6lxi.1.A, 6lxk.1.A, 6nn9.1.A, 6pzf.1.A, 6pzw.1.A, 6q20.1.A, 6q23.1.A, 6v4n.1.A, 6v4o.1.A, 7cm1.1.A

465

466 **Table S1 | Potential "original" epitopes targeted by αEp9 Abs**

Construct #	Pathogen	Target protein	Accession No.	Residues	Epitope sequences	Similarity %
Phage-displayed constructs						**template: Ep9 or EpNeu**
1	SARS-COV-2 (Ep9)	Nucleocapsid	QQX29443.1	152-172	ANNAAIVLQLPQGTTLPKGFY	-
2	SARS-COV-1	Nucleocapsid	YP_009825061.1	153-173	NNNAATVLQLPQGTTLPKGFY	90.5
3	MERS	Nucleocapsid	YP_009047211.1	141-151	NNDSAIVTQFAPGTKLPKNFH	66.7
4	Human coronavirus HKU1	Nucleocapsid	YP_173242.1	166-186	TTQEAIPTRFPPGTILPQGYY	57.1
5	Human coronavirus NL63	Nucleocapsid	YP_003771.1	119-136	NQKPLEPKFSIALPPELS	13.8
6	Human coronavirus OC43	Nucleocapsid	YP_009555245.1	167-187	SSDEAIPTRFPPGTVLPQGYY	71.4
7	Human coronavirus 229E	Nucleocapsid	AGW80953.1	122-138	SEPEIPHFNQKLPNGVT	21.4
8	Human adenovirus 61	Hexon	AQQ81927.1	123-164	ANNAATPQVVFYTEDVNLEMPDTHLVFKPAVPNGTIASESLL	17.6
9	Human mastadenovirus E	PVIII	YP_068038.1	76-114	AALVYQEIPQPTTVLLPRDAQAEVQLTNSGVQLAGGATL	31
10	Influenza A virus (A/Utah/40/2017)	PB2 polymerase	AVH77902.1	225-244	GSVYIEVLHLTQGTCWEQMY	41.7
11	Influenza A virus (EpNeu) (A/Para/128982-IEC/2014(H3N2)	Neuraminidase, partial	AIX95025.1	34-46	ALGQGTTLSKGHS	38.1
12	Influenza B virus (B/California/88/2019)	Neuraminidase	QIA55965.1	67-79	ATKGVVLLLPEPE	28.6
13	Influenza C virus (C/Singapore/DSO-070193/2006)	Polymerase PB1, partial	AFV68302.1	119-145	AATALQLTVDAIKETEGPFKGTTMLEY	34.4
14	Human respiratory syncytial virus A	Fusion protein	ASU44644.1	87-100	NNAVTELQLLMQST	38.1
15	Human respiratory syncytial virus A	Attachment glycoprotein	ART28426.1	106-116	GTTPQSTTIPA	28.6
16	Human metapneumovirus	Nucleoprotein, partial	ABO15448.1	11-33	TTTAVTPSSLPQEITLLCGEILY	34.8
17	Human metapneumovirus	Attachment glycoprotein, partial	AEW90340.1	57-72	PQQTTDKHTALPKSIY	30.8
18	Human betaherpesvirus 6A	Immediate Early protein 2	AGJ52064.1	1396-1422	AATPIDFVGAVKTCNKYAKDNPKEIVL	10
19	Verrucomicrobia bacterium	NADH-quinone oxidoreductase (NOX)	PYJ45937.1	76-89	AGVVLQLPQGTTL	57.1

467

468

20	Clostridium butyricum	Bifunctional methylenetetrahydrofolate dehydrogenase/methenyltetrahydrofolate cyclohydrolase (MTHFD2)	MBE6063617.1	94-104	IILQLPLPKKF	**47.6**
21	Fusobacterium mortiferum	Type II secretion protein	WP_118233983.1	77-99	VENGAIVLQYDKEIYLGLTENFF	**48**
22	Fusobacterium mortiferum	Autotransporter outer membrane protein	WP_005886362.1	449-460	NGAIVGDLVQGT	**38.1**
23	Influenza A virus (A/swine/Missouri/A01774733/2016(H1N2) or A/Para/129501-IEC/2014(H3N2))	Neuraminidase	ANK78229.1 / AIX95013	133-145/ 24-36	ALGQGTTLSNGHS	**92.3**
24	Influenza A (A/swine/Minnesota/A01394278/2013(H3N2))	Neuraminidase	AHA57095.1	134-146	ALGQGTTLNNGHS	**92.3**
25	Influenza A virus (A/California/04/2009 (H1N1))	Neuraminidase	AJI76397.1	75-89	TFFLTQGALLNDKHS	**46.7**
26	Influenza A virus (A/California/111/2015(H3N2))	Neuraminidase	ANM97445.1	133-145	ALGQGTTLNNVHS	**84.6**
27	Influenza A virus (A/mallard/California/1156/2010(H4N6))	Neuraminidase	AEK50939.1	133-142	ALSQGTTLKG	**84.6**
28	Influenza A virus (A/California/33/2011(H3N2))	Neuramidase	AGL06761.1	133-145	ALGQGTTLSNVHS	**84.6**
29	Influenza A virus (**EpNeu Pred**) (A/Para/128982-IEC/2014(H3N2))	Neuraminidase, partial	AIX95025.1	34-56	ALGQGTTLSKGHSNNTVRDRTPY	**-**
eGFP-fusion constructs						
30	Influenza A virus (**EpNeu**) (A/Para/128982-IEC/2014(H3N2))	Neuraminidase	AIX95025.1	34-46	ALGQGTTLSKGHS	**-**
31	Influenza A virus (**EpNeu Pred**) (A/Para/128982-IEC/2014(H3N2))	Neuraminidase	AIX95025.1	34-56	ALGQGTTLSKGHSNNTVRDRTPY	**-**

469

bioRxiv preprint doi: https://doi.org/10.1101/2021.05.21.445201; this version posted June 9, 2021. The copyright holder for this preprint (which was not certified by peer review) is the author/funder. All rights reserved. No reuse allowed without permission.

470 **Table S2 | Primers used to subclone potential original epitopes**

Construct #	Primer names:	Oligonucleotide sequence
Phage-displayed constructs		
	primer_1_F	tcaagggactaccttgcccaaggggttctatGGTGGAGGATCCGGGAGC
1	primer_1_R	ggtaattgtaacacgattgcagcgttattagcTCCACTTCCTTTATCATCGTCATCTTTATAATC
	primer_2_F	acttccacagggaacgacactgccaaagggatttGGTGGAGGATCCGGGAGC
2	primer_2_R	tgcagtacagtggcagcattgttatttccacttccTTTATCATCGTCATCTTTATAATCAACCAATGC
	primer_3_F	tccgggtacaaagttaccaaagaacttccacGGTGGAGGATCCGGGAGC
3	primer_3_R	gcaaattgagtaactatcgctgaatcattgttTCCACTTCCTTTATCATCGTCATCTTTATAATC
	primer_4_F	tcccggaactattttaccccaaggatactatGGTGGAGGATCCGGGAGC
4	primer_4_R	gggaatctagtgggaatcgcctcctgagtagtTCCACTTCCTTTATCATCGTCATCTTTATAATC
	primer_5_F	agtattgccttgccacctgagttatctGGTGGAGGATCCGGGAGC
5	primer_5_R	aaatttcggttcaagcggcttttgattTCCACTTCCTTTATCATCGTCATCTTTATAATC
	primer_6_F	tccgggtactgttttgcctcagggttactacGGTGGAGGATCCGGGAGC
6	primer_6_R	ggaaaccgcgttgggatggcctcatcagagctTTTATCATCGTCATCTTTATAATCAACCAATGC
	primer_7_F	ccagaaattgccgaacggcgttactGGTGGAGGATCCGGGAGC
7	primer_7_R	ttaaagtgagggatctctggctcgctTTTATCATCGTCATCTTTATAATCAACCAATGC
	primer_8_F	TTCTAAATTCACATCCTCAGTATAGAACACGACTTGTGGGGTTGCTGCATTGTTGGCTTTATCATCGTCATCTTTATAATCAACCAATGC
8	primer_8_R	ATGCCAGATACTCATTTGGTCTTCAAACCTGCGGTCCCGAATGGCACGATTGCTAGTGAATCTCTCCTCggtggaggatccgggagc
	primer_9_F	ACGCGGGAGCAGCACTGTAGTCGGCTGAGGGATTTCCTGGTACACCAGGGCGGCTTTATCATCGTCATCTTTATAATCAACCAATGC
9	primer_9_R	GACGCGCAAGCCGAGGTCCAGTTGACAAACAGCGGTGTACAATTGGCTGGCGGTGCCACTCTGggtggaggatccgggagc
	primer_10_F	acacaaggcacttgctgggagcaaatgtatGGTGGAGGATCCGGGAGC
10	primer_10_R	gaggtgcagcacttcaatatagactgacccTTTATCATCGTCATCTTTATAATCAACCAATGC
	primer_11_F	gctttctaagggccacagcGGTGGAGGATCCGGGAGC
11	primer_11_R	gtggtgccttggcccaatgcTTTATCATCGTCATCTTTATAATCAACCAATGC
	primer_12_F	gctgcttccggagccagagGGTGGAGGATCCGGGAGC
12	primer_12_R	agcacgacgcctttcgtagcTTTATCATCGTCATCTTTATAATCAACCAATGC
	primer_13_F	gactgaaggtccttttaagggcacgacaatgttggaatatGGTGGAGGATCCGGGAGC
13	primer_13_R	tctttaatggcatcgaccgtaagttggagagccgtcgctgcTTTATCATCGTCATCTTTATAATCAACCAATGC
	primer_14_F	caactcctcatgcagtctacaGGTGGAGGATCCGGGAGC
14	primer_14_R	aagttctgtgacagcattgttTTTATCATCGTCATCTTTATAATCAACCAATGC
	primer_15_F	gacaaccatccctgcaGGTGGAGGATCCGGGAGC
15	primer_15_R	gattgaggcgtagtcccTTTATCATCGTCATCTTTATAATCAACCAATGC
	primer_16_F	ggaaatcactctcttgtgcggcgaaatcttatatGGTGGAGGATCCGGGAGC
16	primer_16_R	tgcggcaggctagatggcgtaactgccgtagtagtTTTATCATCGTCATCTTTATAATCAACCAATGC
	primer_17_F	acggcactgccgaagtccatctacGGTGGAGGATCCGGGAGC
17	primer_17_R	atgcttgtcagtggtctgttgtggTTTATCATCGTCATCTTTATAATCAACCAATGC
	primer_18_F	caacaaatacgctaaggacaatccgaaagagatcgtgcttGGTGGAGGATCCGGGAGC
18	primer_18_R	caggtcttgacagctccgacgaagtcgatgggcgtagccgcTTTATCATCGTCATCTTTATAATCAACCAATGC
	primer_19_F	tccacaaggcaccacccttGGTGGAGGATCCGGGAGC
19	primer_19_R	agctgcagcacgacgccggcTTTATCATCGTCATCTTTATAATCAACCAATGC
	primer_20_F	gttacctaagaaattcGGTGGAGGATCCGGGAGC
20	primer_20_R	ggaagctgcaaaataatTTTATCATCGTCATCTTTATAATCAACCAATGC
	primer_21_F	agagatttacctggggctgacagagaactttttGGTGGAGGATCCGGGAGC
21	primer_21_R	ttgtcgtactgtaatacaattgcgccgttctccacTTTATCATCGTCATCTTTATAATCAACCAATGC
	primer_22_F	gatttagtacagggtaccGGTGGAGGATCCGGGAGC
22	primer_22_R	gcctacaatggcaccattTTTATCATCGTCATCTTTATAATCAACCAATGC
	primer_23_F	CGCTTTCTAAtGGCCACAGCG
23	primer_23_R	TGGTGCCTTGGCCCAATG
	primer_24_F	CACCACGCTTaacaatGGCCACAGCG
24	primer_24_R	CCTTGGCCCAATGCTTTAT
	primer_25_F	tcttttgaacgacaagcattcaGGTGGAGGATCCGGGAGC
25	primer_25_R	gctccctgagtcagaaagaatgtTTTATCATCGTCATCTTTATAATCAACCAATGC
	primer_26_F	attaaataacgttcatagtGGTGGAGGATCCGGGAGC
26	primer_26_R	gtagtaccctggcccaaggcTTTATCATCGTCATCTTTATAATCAACCAATGC
	primer_27_F	tgcgaacggtacgattcatgatcgttccccattcGGTGGAGGATCCGGGAGC
27	primer_27_R	tgacgacctttcagtgtcgtgccttgagataacgcTTTATCATCGTCATCTTTATAATCAACCAATGC
	primer_28_F	tttgtcgaatgtacactccGGTGGAGGATCCGGGAGC
28	primer_28_R	gtggtaccctggccaagagcTTTATCATCGTCATCTTTATAATCAACCAATGC
	primer_29_F	ctcgaacaacaccgttcgcgaccgtactccgtacGGTGGAGGATCCGGGAGC
29	primer_29_R	tgccctttagacagagttgtcccttggcccaaagcTTTATCATCGTCATCTTTATAATCAACCAATGC
eGFP-fusion constructs		
	primer_30_F	gctttctaagggccacagcAGCGGAAGTGGAGATTATAAAGATGAC
30	primer_30_R	gtggtgccttggcccaatgcGGAGCTCCCGGATCCTCC
	primer_31_F	ctcgaacaataccgtccgcgatcggactccgtacAGCGGAAGTGGAGATTATAAAGATGAC
31	primer_31_R	tgaccttgctcaaagtagtaccctgcccaagcgcGGAGCTCCCGGATCCTCC

bioRxiv preprint doi: https://doi.org/10.1101/2021.05.21.445201; this version posted June 9, 2021. The copyright holder for this preprint (which was not certified by peer review) is the author/funder. All rights reserved. No reuse allowed without permission.

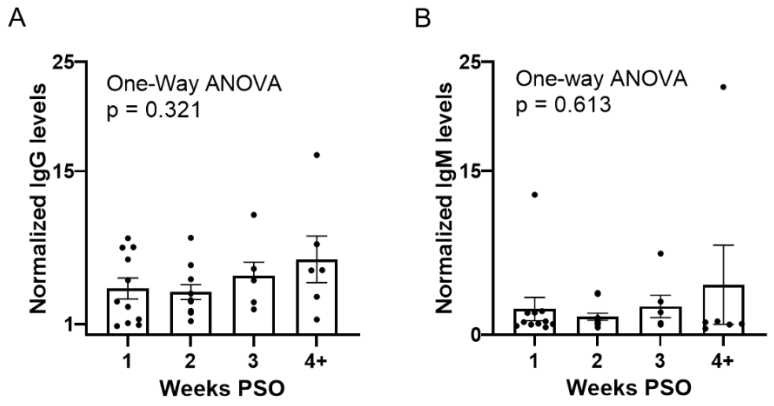

Figure S1 | Early upregulation of αEp9 IgGs. ELISA of αEp9 (**A**) IgG and (**B**) IgM levels in αEp9(+) patients (n = 34) from plasma collected at the indicated time periods post-symptom onset (PSO). Statistical analysis was conducted using one-way ANOVA, *ad hoc* Tukey test. Error bars represent SEM.

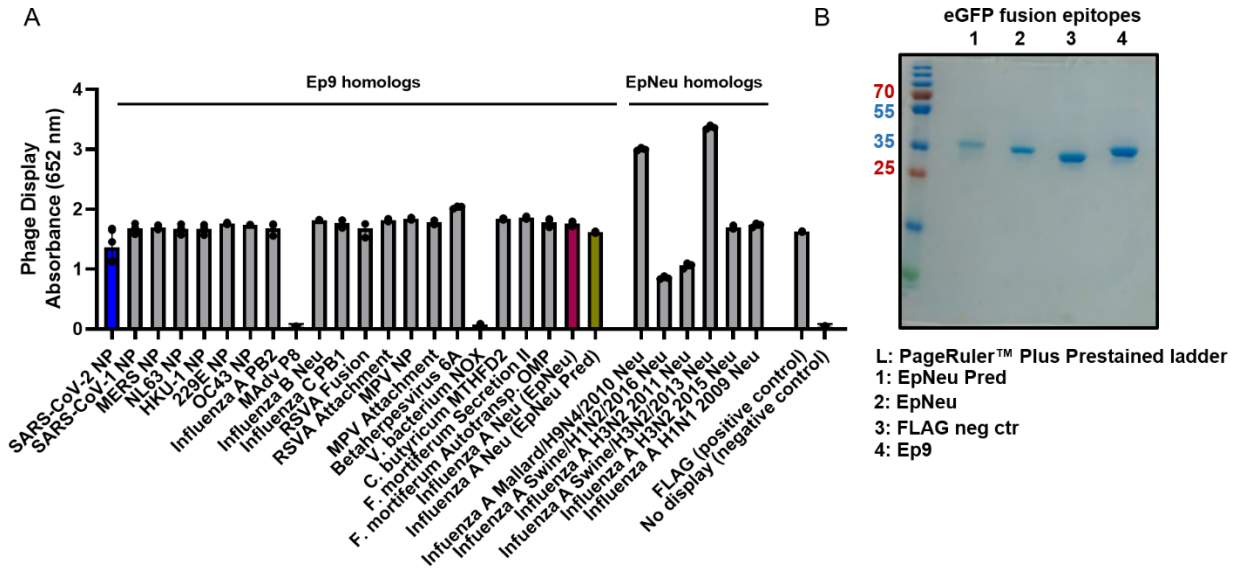

Figure S2 | Expression of phage-displayed and eGFP-fused potential AIM epitopes. (**A**) ELISA demonstrating the display of N-terminal FLAG-tagged potential epitopes fused to the N-terminus of the P8 coat protein. Immobilized αFLAG Abs in microtiter wells bind the displayed FLAG-tag and epitope, and binding is detected with αM-13-HRP Abs as usual. Phage with no epitope displayed provide the negative control. Epitopes for mastadenovirus protein (mAdV) P8 and *V. bacterium* NADH oxidoreductase (NOX) did not display. Error bars represent SD values. (**B**) 10% SDS-PAGE gel stained with Coomassie Blue shows His-tag affinity-purified and buffer-exchanged eGFP-fused epitopes, EpPred, EpNeu, FLAG negative control and Ep9.

bioRxiv preprint doi: https://doi.org/10.1101/2021.05.21.445201; this version posted June 9, 2021. The copyright holder for this preprint (which was not certified by peer review) is the author/funder. All rights reserved. No reuse allowed without permission.

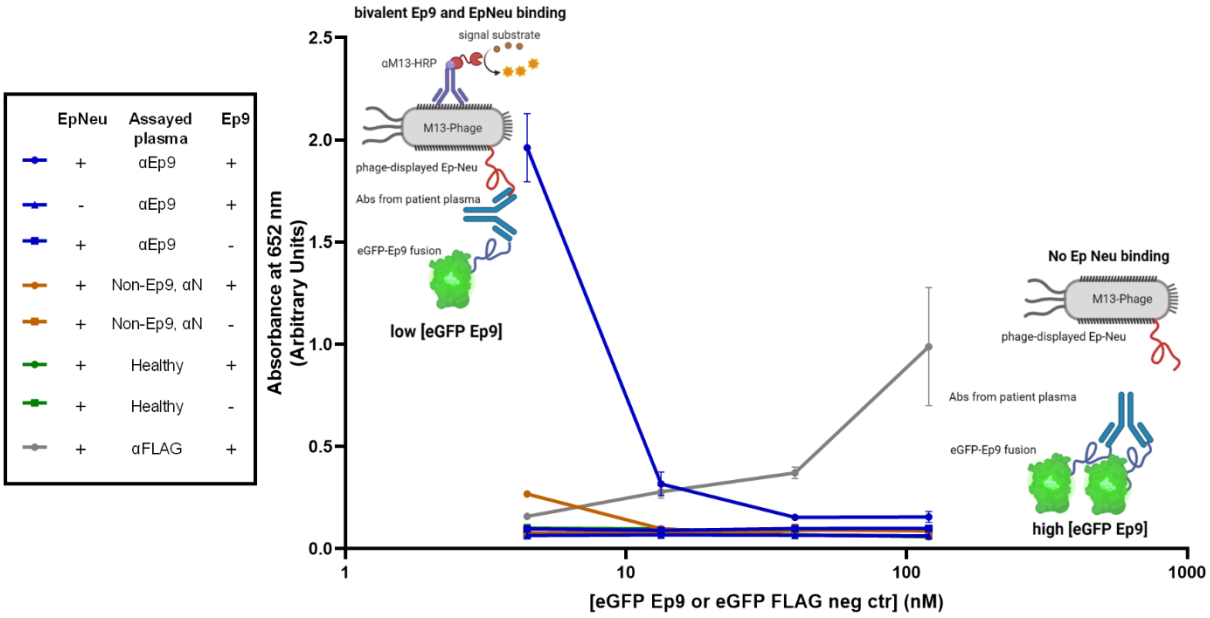

Figure S3 | Optimization of assay to determine cross-reactivity of αEp9 Ab to Ep9 and EpNeu. Sandwich ELISA testing the binding of Abs from the pooled plasma of five αEp9(+) patients, five αEp9(-) patients with other αNP Abs and healthy individuals. This experiment examines bivalent binding to various doses of immobilized eGFP-fused Ep9 epitope (120, 40, 13 and 4 nM) and phage-displayed EpNeu in solution. The data shows that Abs from αEp9(+) patients, but not αEp9(-) or healthy individuals, bivalently bind both EpNeu and Ep9. The positive control (αFLAG 1:2000 fold dilution) at 100 nM eGFP demonstrates concentrations appropriate for bivalent binding to immobilized and in-solution tags. The schematic diagram illustrates the binding observed for bivalence in αEp9 Abs, where the antibody bridges plate-bound eGFP at its high concentrations. Therefore, Figure 2 in the main text uses 4 nM of eGFP Ep9 coated on the plate, and the FLAG positive control uses eGFP at 100 nM. Error bars represent SD.

bioRxiv preprint doi: https://doi.org/10.1101/2021.05.21.445201; this version posted June 9, 2021. The copyright holder for this preprint (which was not certified by peer review) is the author/funder. All rights reserved. No reuse allowed without permission.

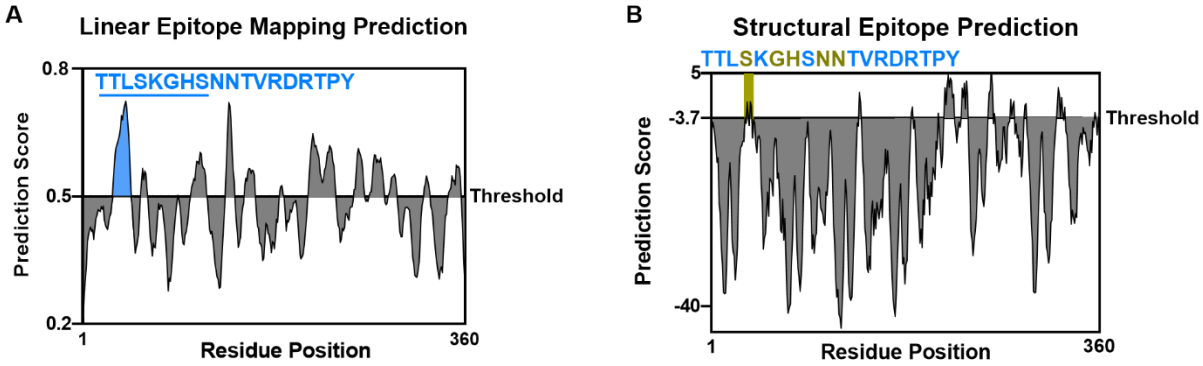

Figure S4 | Linear and structural epitope mapping prediction of Influenza A H3N2 Neuraminidase. (**A**) Linear epitope mapping prediction of the Flu A 2014 H3N2 using Bepipred 2.0[13] demonstrates high prediction scores in a region spanning 18 residues, which includes eight residues from EpNeu (underlined). The additional 10 predicted residues were included as part of an extended epitope termed EpPred. (**B**) Structural epitope mapping, using Discotope 2.0[16], of the modelled neuraminidase protein from Flu A 2014 H3N2 (SWISS-model[21]), predicts an epitope of five residues. These were captured by EpPred, including three found in EpNeu.

bioRxiv preprint doi: https://doi.org/10.1101/2021.05.21.445201; this version posted June 9, 2021. The copyright holder for this preprint (which was not certified by peer review) is the author/funder. All rights reserved. No reuse allowed without permission.

References

1. Fierz, W. & Walz, B. Antibody Dependent Enhancement Due to Original Antigenic Sin and the Development of SARS. *Front. Immunol.* **11**, 1120 (2020).
2. Brown, E. L. & Essigmann, H. T. Original Antigenic Sin: the Downside of Immunological Memory and Implications for COVID-19. *mSphere* **6**, (2021).
3. Kohler, H. & Nara, P. A Novel Hypothesis for Original Antigenic Sin in the Severe Disease of SARS-CoV-2 Infection. *Monoclonal Antibodies in Immunodiagnosis and Immunotherapy* **39**, 107–111 (2020).
4. Ng, K. W. *et al.* Preexisting and de novo humoral immunity to SARS-CoV-2 in humans. *Science (80-.).* **370**, 1339–1343 (2020).
5. Anderson, E. M. *et al.* Seasonal human coronavirus antibodies are boosted upon SARS-CoV-2 infection but not associated with protection. *medRxiv* **7**, 2020.11.06.20227215 (2020).
6. Focosi, D. *et al.* Previous humoral immunity to the endemic seasonal alphacoronaviruses NL63 and 229E is associated with worse clinical outcome in COVID-19 and suggests original antigenic sin. *Life* **11**, (2021).
7. Shrock, E. *et al.* Viral epitope profiling of COVID-19 patients reveals cross-reactivity and correlates of severity. *Science (80-.).* eabd4250 (2020). doi:10.1126/science.abd4250
8. Wang, L. *et al.* Serological Responses to Human Virome Define Clinical Outcomes of Italian Patients Infected with SARS-CoV-2. *medRxiv Prepr. Serv. Heal. Sci.* (2020). doi:10.1101/2020.09.04.20187088
9. Sen, S. R. *et al.* Predicting COVID-19 Severity with a Specific Nucleocapsid Antibody plus Disease Risk Factor Score. *mSphere* **6**, e00203-21 (2021).
10. Altschul, S. F. *et al.* Gapped BLAST and PSI-BLAST: A new generation of protein database search programs. *Nucleic Acids Research* **25**, 3389–3402 (1997).
11. Madej, T. *et al.* MMDB and VAST+: Tracking structural similarities between macromolecular complexes. *Nucleic Acids Res.* **42**, (2014).
12. World Health Organization. WHO | Cumulative Number of Reported Probable Cases of Severe Acute Respiratory Syndrome (SARS). *WHO* 9–11 (2013). Available at: http://www.who.int/csr/sars/country/en/. (Accessed: 16th May 2021)
13. Jespersen, M. C., Peters, B., Nielsen, M. & Marcatili, P. BepiPred-2.0: Improving sequence-based B-cell epitope prediction using conformational epitopes. *Nucleic Acids Res.* **45**, W24–W29 (2017).
14. Gentles, L. E., Wan, H., Eichelberger, M. C. & Bloom, J. D. Antibody neutralization of an influenza virus that uses neuraminidase for receptor binding. *Viruses* **12**, 2020.05.08.084954 (2020).
15. Studer, G. *et al.* ProMod3 - A versatile homology modelling toolbox. *PLoS Comput. Biol.* **17**, (2021).
16. Kringelum, J. V., Lundegaard, C., Lund, O. & Nielsen, M. Reliable B Cell Epitope Predictions: Impacts of Method Development and Improved Benchmarking. *PLoS Comput. Biol.* **8**, (2012).
17. Lipničanová, S., Chmelová, D., Godány, A., Ondrejovič, M. & Miertuš, S. Purification of viral neuraminidase from inclusion bodies produced by recombinant Escherichia coli. *J. Biotechnol.* **316**, 27–34 (2020).

bioRxiv preprint doi: https://doi.org/10.1101/2021.05.21.445201; this version posted June 9, 2021. The copyright holder for this preprint (which was not certified by peer review) is the author/funder. All rights reserved. No reuse allowed without permission.

18. Xie, H. *et al.* H3N2 Mismatch of 2014-15 Northern Hemisphere Influenza Vaccines and Head-to-head Comparison between Human and Ferret Antisera derived Antigenic Maps. *Sci. Rep.* **5**, 1–10 (2015).
19. Flannery, B. *et al.* Enhanced Genetic Characterization of Influenza A(H3N2) Viruses and Vaccine Effectiveness by Genetic Group, 2014-2015. in *Journal of Infectious Diseases* **214**, 1010–1019 (Oxford University Press, 2016).
20. Letunic, I. & Bork, P. Interactive Tree of Life (iTOL) v4: Recent updates and new developments. *Nucleic Acids Res.* **47**, W256–W259 (2019).
21. Waterhouse, A. *et al.* SWISS-MODEL: Homology modelling of protein structures and complexes. *Nucleic Acids Res.* **46**, W296–W303 (2018).
22. Benchling, I. Benchling [Biology Software]. *Retrieved from https://benchling.com* (2017).
23. Levin, A. M. Exploring the interaction between the protein kinase A catalytic subunit and caveolin-1 scaffolding domain with shotgun scanning, oligomer complementation, NMR, and docking. *Protein Sci.* **15**, 478–486 (2006).
24. Pastorino, B., Touret, F., Gilles, M., de Lamballerie, X. & Charrel, R. N. Heat inactivation of different types of SARS-CoV-2 samples: What protocols for biosafety, molecular detection and serological diagnostics? *Viruses* **12**, 735–743 (2020).
25. Mukaka, M. M. Statistics corner: A guide to appropriate use of correlation coefficient in medical research. *Malawi Med. J.* **24**, 69–71 (2012).